Exploring the role of snow metamorphism on the isotopic composition of the surface snow at EastGRIP

Romilly Harris Stuart[1,4], Anne-Katrine Faber[2], Sonja Wahl[2], Maria Hörhold[3], Sepp Kipfstuhl[3], Kristian Vasskog[4], Melanie Behrens[3], Alexandra Zuhr[5,6], and Hans Christian Steen-Larsen[2]

[1]Laboratoire des Sciences du Climat et de l'Environnement, UMR8212, CNRS – Gif sur Yvette, France
[2]Geophysical Institute, University of Bergen and Bjerknes Centre for Climate Research, Bergen, Norway
[3]Alfred-Wegener-Institut Helmholtz-Zentrum für Polar- und Meeresforschung, Bremerhaven, Germany
[4]Department of Geography, University of Bergen, and Bjerknes Centre for Climate Research, Bergen, Norway
[5]Alfred-Wegener-Institut Helmholtz Zentrum für Polar- und Meeresforschung, Research Unit Potsdam, Telegrafenberg A45, 14473 Potsdam, Germany
[6]University of Potsdam, Institute of Geosciences, Karl-Liebknecht-Str. 24-25, 14476 Potsdam-Golm, Germany

Correspondence: Romilly Harris Stuart (romilly.harris-stuart@lsce.ipsl.fr)

Abstract.

Stable water isotopes from polar ice cores are invaluable high-resolution climate proxy records. Recent studies have aimed to improve ~~knowledge~~ understanding of how the climate signal is stored in the stable water isotope record by addressing the influence of post-depositional processes on the surface snow isotopic composition. In this study, the relationship between ~~changes in surface snow microstructure after precipitation/deposition events~~ surface snow metamorphism and water isotopes during precipitation-free periods is explored using measurements of snow specific surface area (SSA). Continuous daily SSA measurements from the East Greenland Ice Core Project site (EastGRIP) situated in the accumulation zone of the Greenland Ice Sheet during the summer seasons of 2017, 2018 and 2019, are used to develop an empirical decay model to describe events of rapid decrease in SSA, ~~driven predominantly by vapour diffusion in the pore space and atmospheric vapour exchange. The SSA decay model is~~ linked to snow metamorphism. We find that SSA decay during precipitation-free periods at EastGRIP is best described by the exponential equation ~~$SSA(t) = (SSA_0 - 26.8)e^{-0.54t} + 26.8$. The model performance is optimal for daily mean values of surface temperature in the range 0 °C to -25 °C and wind speed $< 6\,\mathrm{m\,s^{-1}}$. The findings from the SSA analysis are used to explore the influence of surface snow metamorphism on altering the isotopic composition of surface snow. It is found that rapid SSA decay events correspond to decreases in d-excess over a 2-day period in 72 % of the samples. Detailed studies~~ $SSA(t) = (SSA_0 - 22) \cdot e^{-\alpha t} + 22$, and has a dependency on temperature and wind-speed. The relationship between surface snow SSA and snow isotopic composition is primarily explored using Empirical Orthogonal Function ~~(EOF) analysisrevealed a coherence between the dominant mode of variance of SSA and d-excess during periods of low spatial variability of surface snow over the sampling transect~~analysis. A coherence between SSA and d-excess is apparent during 2017 and 2019, suggesting that processes driving change in SSA also influence ~~d-excess. Our findings highlight the need for future studies to decouple the processes driving surface snow metamorphism in order to quantify the fractionation effect of individual processes on the snow isotopic composition.~~ snow isotopic composition. In contrast, 2018 was characterised by a covariance between SSA and $\delta^{18}O$ highlighting the inter-annual variability in surface regimes. Moreover, we observed

changes in isotopic composition consistent with fractionation effects associated with sublimation and vapour diffusion during periods of rapid decrease in SSA. Our findings support recent studies which provide evidence of isotopic fractionation during sublimation.

1 Introduction

The traditional interpretation of stable water isotopes in ice cores is based on the linear relationship between local temperature and ~~first order~~ first-order parameters δ^{18}O and δD of surface snow on ice sheets (Dansgaard, 1964). ~~The second order parameter d-excess (d-excess = δD - 8 · δ^{18}O) is a result of kinetic fractionation caused by different molecular diffusivities of oxygen and hydrogen and has traditionally been interpreted in ice core records as reflecting moisture source conditions (Merlivat and Jouzel, 1979). Many factors must be accounted for when reconstructing temperature in ice cores, including~~ Accurate reconstruction requires consideration of precipitation intermittency (Casado et al., 2020; Laepple et al., 2018), past variations in ice-sheet elevation (Vinther et al., 2009), sea ice extent (Faber et al., 2017; Sime et al., 2013), and firn diffusion (Johnsen et al., 2000; Landais et al., 2006; Holme et al., 2018)~~. In addition, recent~~ , which influence the water isotopic composition in ice cores. The second-order parameter deuterium excess (d-excess) is defined by the deviation from the near-linear relationship between δ^{18}O and δD which is driven by non-equilibrium (kinetic) fractionation (d-excess $= \delta\text{D} - 8 \cdot \delta^{18}\text{O}$). d-excess in ice cores is understood to reflect moisture source conditions (Dansgaard, 1964; Merlivat and Jouzel, 1979; Johnsen et al., 1989) , changes in moisture source region (Masson-Delmotte et al., 2005), and can be modified during snow crystal formation in supersaturated clouds (Ciais and Jouzel, 1994; Sodemann et al., 2008).

Recent studies have documented isotopic composition change in the surface snow during precipitation-free periods (Steen-Larsen et al., 2014; Ritter et al., 2016; Casado et al., 2018; Hughes et al., 2021), linked to synoptic variations in atmospheric water vapour composition and subsequent ~~snow-vapour exchange (Steen-Larsen et al., 2014). Current research aims to quantify the influence of post-depositional processes on isotopic change~~ exchange with the surface snow (Steen-Larsen et al., 2014; Ritter et al., 201 . Post-depositional processes at the surface involve additional kinetic effects adding complexity to the interpretation of d-excess (Hughes et al., 2021; Casado et al., 2021). Here we focus on processes influencing isotopic composition of the surface snow ~~(Steen-Larsen et al., 2014; Ritter et al., 2016; Madsen et al., 2019; Wahl et al., 2021)~~after deposition while exposed to surface processes and concentrate on the second order parameter d-excess.

~~Surface snow undergoes structural changes , as grains form bonds, grow. This process is called~~ After deposition, snow grains undergo structural changes known as snow metamorphism, which is active at the surface and at greater depths, depending on temperature (gradient) conditions ~~(Colbeck, 1983; Pinzer and Schneebeli, 2009b). A major change the snow is undergoing, is the reduction of the ice-air interface to reduce energy (Legagneux and Domine, 2005)~~(Colbeck, 1983; Pinzer and Schneebeli, 2009a) . Surface snow metamorphism is initially driven by a reduction in the snow-air interface to reach thermodynamic stability (Colbeck, 1980; Legagneux and Domine, 2005). The snow-air interface can be described by the widely used parameter ~~SSA. It is assumed to be linked to the optical grain size equivalent (Linow et al., 2012) and can be utilized~~ snow specific surface area (SSA), which is dependent on optical grain radius and density of ice ($SSA = 3/\rho_{ice} \cdot r_{opt}$) (Gallet et al., 2009), and can be

used as a measure for snow metamorphism (Cabanes et al., 2002, 2003; Legagneux et al., 2002). ~~In this study we use SSA to describe the (rapid) change of surface snow as one measure for snow metamorphism.~~

~~This manuscript focuses on surface snow property changes after precipitation. We here explicitly refer to snow which is lying at the surface for an unknown amount of time and thus does not directly represent freshly precipitated snow.Fresh snow crystals have a high value of SSA. After deposition of the crystals on the surface~~ Freshly deposited snow has a high SSA which decreases with time under both isothermal (<10 °C m^{-1}) and temperature gradient (>10 °C m^{-1}) conditions within the snow (Cabanes et al., 2002; Legagneux et al., 2004; Domine et al., 2007; Genthon et al., 2017). Decrease in SSA is predominantly the result of Ostwald Ripening, where large grains grow at the cost of smaller grains (Lifshitz and Slyozov,1961; Legegneux et al., ~~the SSA rapidly decreases from its initial value due to crystal growth (Cabanes et al., 2002; Legagneux et al., 2004; Domine et al., 2007~~ ~~. The reasons for the SSA decrease are wind-driven fragmentation (Comola et al., 2017; Neumann et al., 2009), interstitial vapour diffusion in the pore space between snow crystals (Pinzer et al., 2012; Flin and Brzoska, 2008) and sublimation (Sokratov and Golub~~ 2004), interstitial vapour diffusion (Flin and Brzoska, 2008; Sokratov and Golubev, 2009; Pinzer et al., 2012), and wind effects (Picard et al., 2019). Under natural conditions, SSA decrease is driven by a combination of these processes depending on surface conditions (Cabanes et al., 2003; Pinzer and Schneebeli, 2009a), each potentially modifying the isotopic composition of the snow (Ebner et al., 2017).

Models can provide a quantitative description of ~~the rapid~~ SSA decrease after ~~precipitation~~deposition. Previous studies have proposed SSA decay models using a combination of field measurements and controlled laboratory experiments (Cabanes et al., 2002, 2003; Legagneux et al., 2003, 2004; Flanner and Zender, 2006; Taillandier et al., 2007). ~~While current versions of the so-called decay models exist, these are mostly based on lab-experiments and non-polar snow observations.~~ Exponential models are documented to produce the best fit to in-situ SSA decay data (Cabanes et al., 2003). A subsequent physical-based model was defined by Legagneux et al. (2003) to describe SSA decay based on grain growth theory, which was then further developed by Flanner and Zender (2006), who defined parameters based on surface temperature, temperature gradient and snow density. Existing SSA decay models have rarely been applied to polar ice sheet surface snow (Linow et al., 2012; Carmagnola et al., 2013) . Conditions for surface snow on polar ice sheets ~~such as Greenland are however~~ are not necessarily comparable to other alpine ~~regions. The dry-accumulation zone of the Greenland ice sheet has only small amounts of intermittent precipitation. Furthermore, the~~ and Arctic regions due to negligible melt and the high-latitude radiation budget~~is different than in other alpine regions.~~

~~Only few continuous datasets of daily~~ . Moreover, while continuous surface SSA measurements exist from ~~the remote regions of the polar ice sheets (Libois et al., 2014; Picard et al., 2014). While SSA observations from Greenland exist (Carmagnola et al., 2013; Lin~~ ~~, diurnal datasets covering multiple months and years provide a better foundation for~~ Antarctica (Gallet et al., 2011, 2014; Picard et al., 2014 , those from Greenland focus on the depth evolution of SSA (Carmagnola et al., 2013; Linow et al., 2012). Continuous datasets of daily SSA and corresponding isotopic composition measurements from the accumulation zone of the Greenland Ice Sheet can contribute to understanding the relevance of snow metamorphism for ~~ice core studies. In particular, studies of SSA and snow metamorphism from Greenland are relevant for isotope~~ surface energy budget and for ice core studies. ~~This is because snow metamorphism is expected to influence the snow isotopic composition as~~ The latter is of particular interest owing to

observations of isotopic fractionation during snow metamorphism documented in laboratory studies (Ebner et al., 2017) and field experiments ~~(Hughes et al., 2021)~~(Hughes et al., 2021; Wahl et al., 2021; Casado et al., 2021). Nonetheless, few studies have focused on the direct relationship between physical snow properties, such as SSA, and post-depositional changes in isotopic composition.

~~An SSA decay model optimized for Greenland conditions would provide a better quantitative foundation for a process-based understanding of surface snow metamorphism on Greenland. Furthermore, a quantitative description of Greenland SSA decay would provide a basis to explore how snow metamorphism at the surface plays a role for the alteration of isotopic composition of Greenland snow after deposition.~~

In this manuscript, the aim is to explore the behaviour of surface snow metamorphism on polar ice sheets using daily SSA measurements ~~, and compare~~ from Northeast Greenland during summer, and to compare the change in physical properties to the isotopic composition measurements. The primary focus is to document events where changes in SSA occur rapidly over a ~~duration of a few days.~~ number of precipitation-free days, which we use as a proxy for snow metamorphism. ~~We first identify events of rapid SSA decreases (decays) and explore how the isotopic composition of the snow changes during these events. Using daily field observations of snow properties from Northeast Greenland during summer, events of~~ Events of rapid SSA decrease (SSA decay events) are used to 1) quantify and model surface snow metamorphism in polar snow and, 2) assess isotopic change during surface snow metamorphism ~~.~~ in-situ. The data presented here has ~~the potential to contribute to the~~ great value for our understanding of the influence of post-depositional processes on physical and isotopic changes in the polar ice sheet surface snow. This allows for ~~better~~ deeper understanding of snow properties at remote regions of polar ice sheets ~~, and contributes~~ and contributes to the interpretation of water isotopes in polar ice cores.

2 Study site and methods

2.1 EastGRIP site overview and meteorological data

All data used in this paper ~~were~~ was collected as part of the Surface Program corresponding to the international deep ice core drilling project at the East Greenland Ice Core Project site (EastGRIP 75.65°N, 35.99°W; 2,700 m.a.s.l) during summer field seasons (~~May-August~~May-August) of 2017, 2018 and 2019. The local accumulation rate is approximately 14 cm water equivalent per year (Schaller et al., 2017).

Meteorological data used for this study are from the Program for Monitoring of the Greenland Ice Sheet (PROMICE) Automatic Weather Station set up by the Geological Survey of Denmark and Greenland (GEUS) at EastGRIP in 2016 (Fausto et al., 2021). The data are 10-minute mean values for a number of variables. In addition to the surface variables, snow temperature was measured using a thermistor string at 0.1 m intervals during 2017 and 2018 but was modified to 1 m intervals in 2019. An additional thermistor string was thus installed in May of 2019, from which we use the 0.1 m measurements. Relevant weather variables for this study are surface temperature (calculated from longwave radiation down and longwave radiation up with longwave emissivity set at 0.97), air temperature and wind speed (Van As, 2011). Mean weather conditions vary between sampling years, as outlined in Table 1 ~~. Instrument specifics can be found in Fausto et al. (2021). Mean summer surface~~

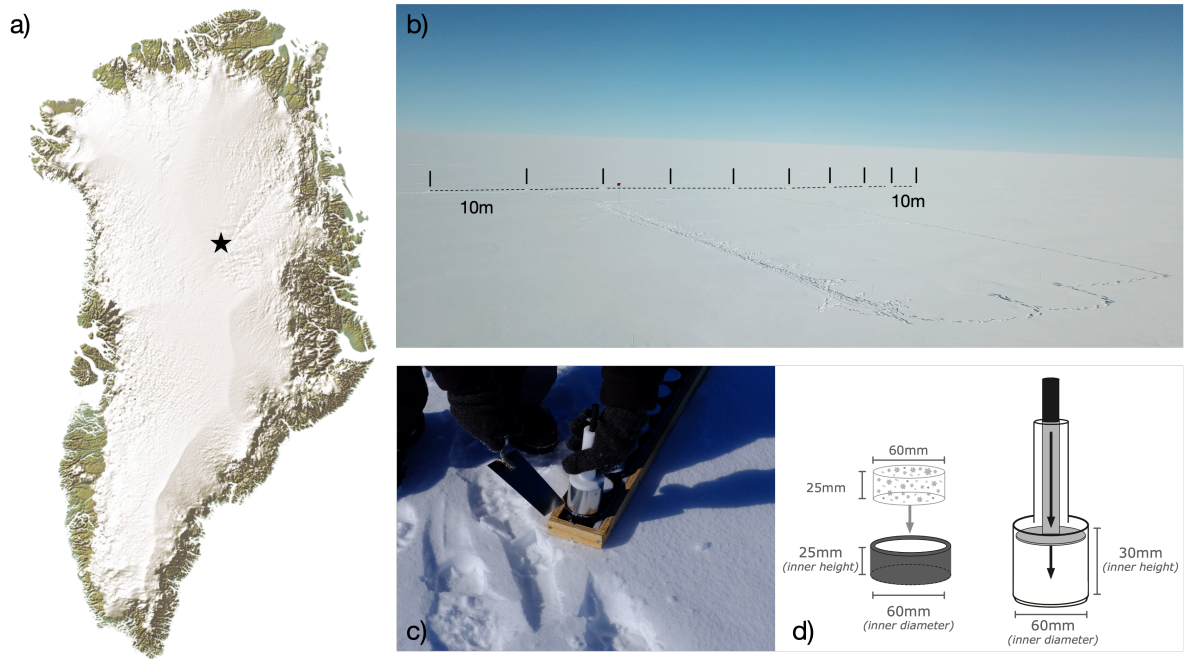

Figure 1. ~~*SSA Sampling Procedure*~~a) A map of Greenland with a black star indicating the EastGRIP site (Source: ~~Eric Gaba – Wikimedia Commons user: Sting~~VisitGreenland). b) A photograph of the clean snow area at the field site (Credit: Bruce Vaughn), ~~with~~ black lines ~~indicating~~ indicate the SSA sampling transect with 10 m spacing shown as dashed lines. c) A photograph of SSA sampling cups (Credit: Sonja Wahl), and d) an illustration of the sampling device from Klein (2014).

~~temperatures for 2019 were -10.6±5 °C, 5 °C higher than 2017 and 2018. Westerly winds prevail, with mean wind speed of 4.5 m s^{-1} (Madsen et al., 2019).~~ with prevailing westerly winds throughout the sampling seasons.

An ~~Eddy-Covariance tower~~ eddy-covariance (EC) measurement tower was set up at EastGRIP ~~in 2016. The relevant variable measured from this system is~~ for every summer observation period (Madsen et al., 2019; Wahl et al., 2021). Here we use the 30-minute latent heat flux (~~LHF) which is directly determined by~~ LE) measurements which are calculated from the measurement of humidity fluxes between the surface and atmosphere. Positive ~~LHF~~ LE indicates upwards energy flux in the form of sublimation in Table 1. ~~All field seasons had net sublimation, with the highest magnitude observed in 2019 (See Data Availability Section A).~~

Significant weather conditions such as ground fog, drifting snow and snowfall, were documented each day in the EastGRIP field diary.

Weather statistics - 2017, 2018 and 2019 The table present the mean

Table 1. Weather statistics - 2017, 2018 and 2019. Mean and standard deviation for the weather variables , surface during the three sampling seasons. Surface temperature, relative humidity with respect reference to ice , wind speed and latent heat flux. Surface temperature and wind speed are from the use PROMICE weather station based on hourly 10-minute measurementsduring the field seasons of 2017, 2018 and 2019. Relative humidity with respect to ice is calculated from vapour pressure of the air and saturation vapour pressure over ice. Latent heat flux is taken a 30-minute mean upwards flux from the EC eddy-covariance towerdataset.

		2017	2018	2019
	Instrument	*06/05 - 05/08*	*04/05 - 07/08*	*24/05 - 01*
Mean Mean Mean height**Surface Temperature** (°C)	(Kipp and Zonen CNR1/CNR4 radiometer)	-14.5 ± 6.2	-15.76 ± 7.6	-10.6 ± 5
Relative Humidity (with respect to ice) (%%)	(Calculated)	96 95.8 ± 15	96 95.9 ± 16	94 93.3 ±
Wind Speed ($m s^{-1}$)	(R.M. Young 05103-5 ±0.3 $m s^{-1}$)	4.9 ±. 2 0.2	4.2 ± 1.9	4.5 ± 1.6
Latent Heat Flux ($W m^{-2}$ $W m^{-2}$)	1.3 (IRGASON Campbell Scientific)	1.28 ± 4 4.2	1.1 1.3 ± 3.9 4.3	2.6 ± 5.9 5

2.2 Snow sampling procedure and snow accumulation

Each summer season of 2017, 2018 and 2019 snow samples were taken once a day, primarily in the morning, from May to August at 10 sampling sites, each . Each site was marked by a stick, along a 90 m transect with 10 m spacing upwind of the EastGRIP camp to ensure clean snow (Fig. 1b). The specific dates for each season are given in Table 1. The precise location of each sample was marked by a small stick to ensure the adjacent snow is sampled the next day and to avoid sampling snow from different depths. A 6 cm diameter sampling device collected the top 2.5 cm of surface snow (Fig. 1c). Snow density is determined using the weight of each snow sample with a known volume. At the start of each season, sticks Sticks were placed at each site and snow heightwas determined by sampling site at the start of each season to measure snow height, that is, the distance between the snow surface and top of the stick . Accumulation with a ruler with an uncertainty margin of ±0.5 cm. Accumulation, used here to describe the change in snow height (cm), was calculated using the cumulative sum of the daily difference between measurements of snow height from each site. The resultant datasets consist of 10 daily measurements of three parameters, SSA, density and accumulation, over a 92, 100 and 66 day period for snow accumulation. The field season for 2018 started on the 5th of May, 9-days earlier than 2017 , 2018 and (14th May), and 22 days earlier than 2019 respectively. (27th May). The meteorological data is re-sampled to the SSA sampling time-periods to ensure consistent comparison.

Although samples were measured each day, the exact sampling time varies. Snow sampled during the afternoon would have had extended time exposed to solar radiation maximum, compared to snow sampled during the morning. Furthermore, the sampling time has implications for capturing precipitation events.

2.3 SSA measurements

2.4 ~~Ice Cube calibration~~

Each snow sample is placed into the Ice Cube sampling container below an Infra-Red (IR) laser diode (1310 nm), where the SSA is calculated based on IR hemispherical reflectance, as explained in Gallet et al. (2009)~~, while~~. More information on the Ice Cube device can be found in Zuanon (2013). ~~Light penetration depth~~ The *e*-folding depth of 1310 nm radiation in snow of 200 kg m^{-3} is approximately 1 cm ~~(Gallet et al., 2011), resulting in a measurement of the top <1~~(Gallet et al., 2009). Thus, as the mean snow density from all field seasons is 293 ~~cm of each sample (Mean snow density at EastGRIP 2017, 2018 and 2019 =~~ kg m^{-3} (307 $\pm$ 40 kg m^{-3}, 278 $\pm$ 47 kg m^{-3}, 294 $\pm$ 50 kg m^{-3} ~~)~~for 2017, 2018 and 2019), each measurement will be heavily weighted towards the top <1 cm of the 2.5 cm sample. The light reflected from the snow samples is converted into inter-hemispheric IR reflectance using a calibration curve based on methane absorption methods (Gallet et al., 2009). A radiative-transfer model is used to retrieve SSA from inter-hemispherical IR reflectance. To avoid influence from solar radiation, SSA was measured inside a ~~ventilated white tent~~ white tent or in a snow cave kept at temperatures between -5 °C and ~~-10~~-20 °C. ~~SSA measurements have~~ We assume an uncertainty of 10~~% for values between 5-130~~% for SSA measurements between 5–130 m^2 kg^{-1} (Gallet et al., 2009).

2.4 Surface snow isotopes

~~Samples collected following the sampling procedure outlined in Section 2.2 were also used for isotopic composition measurements, resulting in~~ Individual SSA samples were put in separate bags and subsequently measured for water isotopic composition. Thus, every day the 10 ~~daily isotope measurements taking~~ SSA samples have a corresponding isotopic composition. The resultant isotope value is the average composition over the top ~~25~~2.5 ~~mm~~ cm of snow. Each sample was ~~sealed in polyethylene bags to avoid any air to equilibrate with the snow and affect the isotopic composition. All samples were~~ kept frozen during transportation and storage.

~~After melting, each bag was shaken to ensure the isotopic composition of the sample is representative. 1.25 μl of each sample was then pipetted into a vial ready for isotopic analysis. The snow~~ The samples were then analysed at ~~Alfed~~ Alfred Wegener Institute in Bremerhaven using a cavity ring-down spectroscopy instrument ~~model~~ (Picarro L-2120-i and L-2140-i) following the protocol of Van Geldern and Barth (2012). This technique ~~is used to obtain measurements of~~ produces δ^{18}O and δD measurements with an uncertainty of 0.15‰ and 0.8‰ respectively. ~~d-excess is calculated by the equation $d-excess = \delta D - 8 \cdot \delta^{18}$O with a resultant~~ The calculated values for *d*-excess have an uncertainty of 1‰. ~~Observing relationships between our SSA and isotope data requires consideration for the depth offset between the SSA measurements and the isotopic composition measurement which measures the entire 2.5 cm snow layer.~~

2.5 Data analysis

2.6 ~~Data analyses~~

2.5.1 Defining SSA decay events

~~This study focuses on the events where the SSA measurements decay rapidly over a duration of a few days. SSA decays are here defined as the~~ Freshly deposited snow has a high SSA that slowly decreases through time due to snow metamorphism. Based on this understanding, two terms are defined: 1) SSA increase indicating deposition events in the form of precipitation, drifted snow or surface hoar formation, and 2) SSA decay due to snow metamorphism and other post-depositional processes such as wind-erosion, where the SSA decreases. Identification of such SSA decays in the time-series are required to quantify snow metamorphism and corresponding isotopic change during precipitation-free periods. Surface conditions are subsequently assessed to remove events where the ~~2-day change of daily mean values are higher than a given threshold. This threshold is the same value for all years and is calculated based on the 10th percentile of the decays and set at -13~~surface snow layer is likely to have experienced perturbation via deposition or erosion.

A threshold is derived to systematically identify periods of rapid SSA decay - hereafter referred to as SSA decay events - over a two-day period which was found to be the most representative time step to capture SSA decay events for all sampling years. SSA decay events captured by this threshold are defined by the peak SSA value (day-0), through to the next increase in SSA (rather than decrease).

A set of criteria are required to reduce the potential of analysing SSA decay events with wind-perturbed surfaces. In Antarctica, unconsolidated surface snow has been observed to drift at wind speeds as low as $5\,m^{2}~kg~s^{-1}$ ~~2-day~~measured at 2 m height (Birnbaum et al., 2010). However, a study from north-east Greenland documented snowdrift starting at $6\,m\,s^{-1}$ (Christiansen, 2001), due to warmer temperatures facilitating bonding of the surface snow (Li and Pomeroy, 1997). Field-diary observations from EastGRIP document snowdrift when wind speeds exceeded $7\,m\,s^{-1}$. ~~If the daily mean changes over a 2-day period is higher than the threshold, then this period is selected as a rapid SSA decay event. The duration of the event is set to start at the rapid decay~~

Based on this assessment, we define two wind-speed categories for comparison of the effects of wind-speed on SSA decay. The first includes events with daily maximum wind-speed below $6\,m\,s^{-1}$, hereafter referred to as low-wind events, with negligible surface perturbation. Secondly, we consider events where the daily maximum wind-speed is between $6–7\,m\,s^{-1}$, hereafter referred to as the moderate-wind events. The inclusion of moderate-wind events facilitates an assessment of the influence of wind-speed on SSA decay, while the threshold wind-speed for snowdrift based on temperature conditions from Li and Pomeroy (1997) is used to ensure minimal chance of drift.

2.5.2 Modelling surface snow metamorphism

The first empirical SSA decay model, Eq.(1), was proposed by Cabanes et al. (2003) who described a temperature-dependent exponential decay based on snow samples collected from the Alps (Cabanes et al., 2002) and Arctic Canada (Cabanes et al., 2003)

. Legagneux et al. (2003) found Eq.(2) to best describe experimental SSA decay under controlled laboratory conditions.

$$SSA(t) = SSA_0 \cdot e^{-\alpha t} \tag{1}$$

$$SSA(t) = B - A \cdot ln(t + \Delta t) \tag{2}$$

Parameters A and B in Eq.(2) were found to be arbitrarily related to the decay rate and initial SSA of each sample. To improve the physical basis of the model, the theory of Ostwald Ripening, describing grain growth driven by thermodynamic instability, was implemented into the model (Legagneux et al., 2004). Eq. (3) has two parameters τ and ~~end on~~ n; τ is the ~~day when the mean SSA measurements increase (rather than decrease)again.~~ decay rate and n relates to theoretical grain growth. The physical model was further developed by Flanner and Zender (2006) to incorporate a physical quantification of the parameters including information about temperature, temperature gradient, and density. Based on these three conditions, they created a look-up table for τ and n.

$$SSA(t) = SSA_0 \cdot \left(\frac{\tau}{t + \tau} \right)^{1/n} \tag{3}$$

2.5.3 ~~Modelling surface snow metamorphism~~

Taillandier et al. (2007) proposed two equations based on Eq. (2) to define the decay rate under isothermal and temperature gradient conditions where they were able to directly incorporate a surface temperature parameter (T_m).

~~An empirical decay model is constructed building~~

$$SSA(t) = [0.659 \cdot SSA_0 - 27.2 \cdot (T_m - 2.03)] - [0.0961 \cdot SSA_0 - 3.44 \cdot (T_m - 1.90)] \cdot (t + e^{\left(\frac{0.659 \cdot SSA_0 - 27.2 \cdot (T_m - 2.03)}{[0.0961 \cdot SSA_0 - 3.44 \cdot (T_m - 1.90)]} \right)}) \tag{4}$$

Building upon previous studies~~(Cabanes et al., 2002, 2003; Flanner and Zender, 2006; Legagneux et al., 2002, 2003; Taillandier et al., 2~~ ~~. This model uses~~ , we define an empirical SSA decay model using continuous daily SSA measurements from EastGRIP to describe the behaviour of surface snow SSA in polar summer conditions (Cabanes et al., 2002, 2003; Flanner and Zender, 2006; Legagneux et . A recent study at EastGRIP has shown the significant heterogeneity in surface snow due to post-depositional reworking from the wind (Zuhr et al., 2021), and therefore each sample is treated individually to avoid signal attenuation. ~~The post-precipitation decreases in SSA are hereafter referred to as decays.~~

$$SSA(t) = SSA_0\, e^{-\alpha t}$$

3 Results

~~Eq. (1) is proposed by Cabanes et al. (2003) as the most accurate description of SSA decay, where SSA_0 is the initial SSA value, α the decay rate. To best describe grain coarsening and the processes of sublimation and deposition driving mass redistribution of a new snow layer, days with mean wind speeds above 6~~

3.1 EastGRIP meteorological conditions

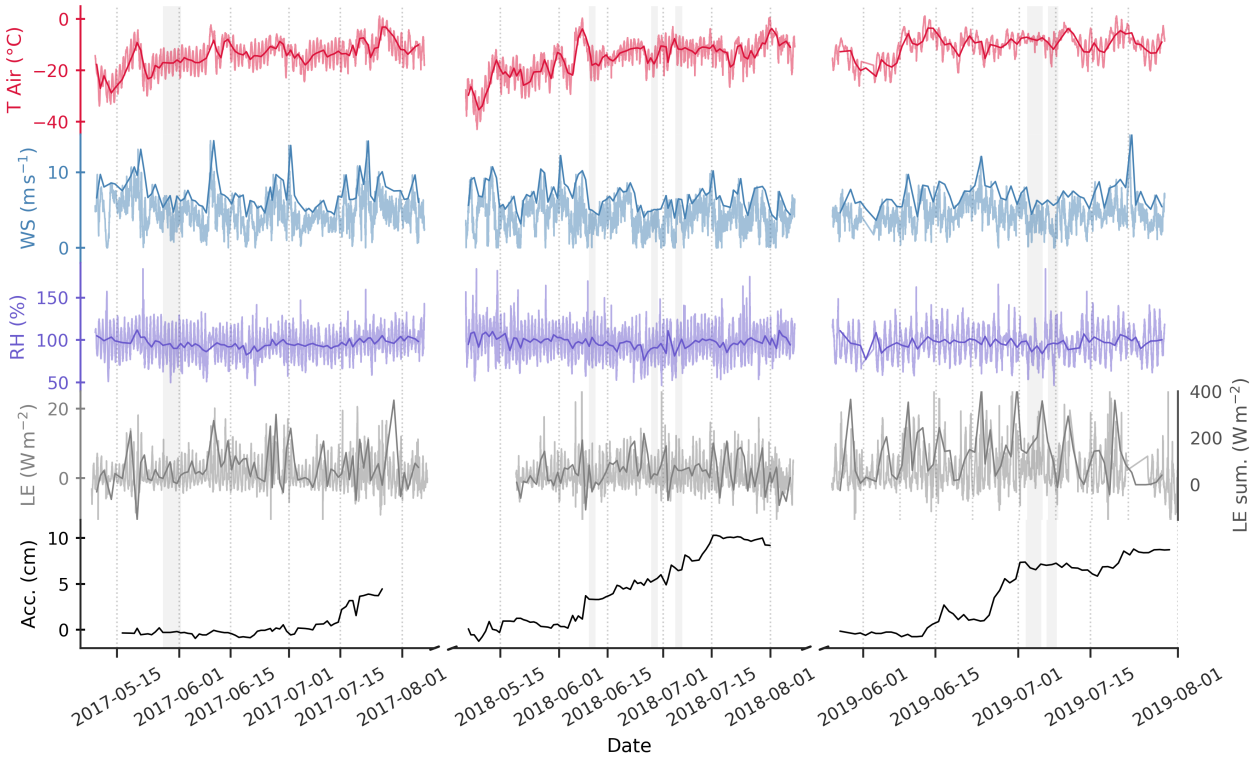

Figure 2. Time series of the ambient conditions during the sampling periods. Data covers the specific sampling periods each year. 10-minute mean data from the AWS is presented for air temperature, wind-speed and relative humidity. Mean values (bold lines) are shown for air temperature and relative humidity, while daily maximum is shown for wind-speed. Latent heat flux data are 30-minute averages from the eddy-covariance tower, with the daily sum shown in bold. Snow accumulation is presented in the lower panel as the daily mean over the 10 sampling sites (see Section 2.2). Grey bars indicate the derived SSA decay events.

Meteorological variables over the three sampling seasons vary substantially as shown in Fig. 2. Air temperatures were below -30 °C between May 5th and May 8th in 2018. Such low temperatures were not recorded for 2017 and 2019. Moreover, when comparing the period from May 27th to August 5th of each year (duration of 2019 season), 2018 air temperatures (-13.3 °C) were still 0.5 °C lower than 2017 and 3.2 °C lower than 2019.

The 2017 season was characterised by high wind intrusions of $>13\,\mathrm{m\,s^{-1}}$ ~~are removed to reduce the influence of wind redistribution. Individual sample analysis is preferentially used to avoid daily mean values possibly attenuating any signals due to spatial variability in surface snow age. Aged snow patches are expected to respond differently to surface processes than new snow patches due to different original crystal structures at the start of events~~at approximately 20-day intervals. Considering all three sampling years, the average daily maximum wind speed is $7\,\mathrm{m\,s^{-1}}$, with 209 out of the total 237 sampling days having maximum wind speed above $5\,\mathrm{m\,s^{-1}}$. The distributions of daily maximum wind-speed compared to 10-minute mean values are found in the Supplemental Fig. A1. Between the start and end of the 2017 field season, we observed net-accumulation of 4.81 cm of snow over the 89-day season, compared to 9.30 cm in 2018 and 8.58 cm in 2019. In addition, the total sum of LE during 2019 was 30% greater than in 2018 indicating strong sublimation. Eddy-covariance LE measurements are supported by LE from AWS observations which indicate the same magnitude of difference between the years.

4 ~~Results~~

3.1 ~~SSA decay events~~

3.0.1 Spatial and temporal snow surface variability

Seasonal variability is observed in SSA, δ^{18}O and *d*-excess throughout the field seasons of 2017, 2018 and 2019 (Fig.3), with highest daily spatial variability in isotopic composition. SSA is characterised by peaks, often corresponding to high spatial variability, followed by gradual decreases over a number of days, the SSA decay feature which is most prominent during 2017 and corresponds to negligible or decreasing accumulation. High SSA values at the start of the 2018 season (daily mean $88\,\mathrm{m^2\,kg^{-1}}$) correspond to low and spatially homogeneous δ^{18}O.

~~SSA data collected at EastGRIP indicate continuous changes in the physical structure of the snow crystals during all sampling seasons~~ Inter-annual difference is observed in δ^{18}O, with seasonal mean values of -31.6 $\pm$ 2.1‰, ~~with both temporal and spatial variability. The temporal SSA variability shows changes in physical snow structure with peak values closely associated with precipitation and decreases due to post-depositional re-working of the snow. Summer seasonal SSA evolution is presented in Fig. ??~~ -32.7 $\pm$ 1.3‰ and -27.3 $\pm$ 2.1‰ for 2017, 2018 and 2019 ~~with each faded line representing individual samples (10 per day), and the bold line showing the daily mean. Spatial variability between sites is most prevalent when there are high SSA values, indicating fresh snow~~respectively (Fig. 3). Throughout the season δ^{18}O follows a gradual increasing trend from May to August following increasing temperatures. Note that the 2019 field season started approximately 15 days later than 2017 and 2018, resulting in a bias towards mid-summer conditions. Cases of abrupt decreases (-10‰) are observed in the late summer, for example, on July 12th in 2018 and July 25th in 2019, which correspond to late-summer snowfall events. No clear seasonal trend is observed in *d*-excess, but rather there are periods of gradual decrease in *d*-excess during periods with no accumulation in all years. The most apparent is from May 15th to June 14th in 2017 corresponding to 0 cm net-accumulation (Fig. 3). The maximum daily spread in δ^{18}O and *d*-excess is approximately 15‰, indicating strong surface heterogeneity.

~~A total of 21 rapid SSAdecay events are identified, with 6, 9 and 6 events for~~ Empirical Orthogonal Function (EOF) analysis is applied to the data to identify the dominant modes of variance in both the temporal and spatial dimensions for each parameter - SSA, $\delta^{18}O$ and *d*-excess. Using a confidence interval of 95% ($p<0.05$), the relationship between SSA and isotopic composition is tested. The spatial and temporal principal components returned for each variable by the EOF are presented in Fig. 3. During 2017, 2018 and 2019 ~~respectively. Grey bars in Fig. ?? highlight events defined by the decrease threshold. Maximum SSA values for 2018 and~~ all variables have one dominant mode of variance, or principal component (PC1). PC1 of SSA ($PC1_{SSA}$) explains 61 %, 77 % and 72 % of variance for the respective years, PC1 of $\delta^{18}O$ ($PC1_{\delta^{18}O}$) explains 69 %, 83 % and 75 % of the total variance respectively, while PC1 of *d*-excess ($PC1_{dxs}$) explains 47 %, 51 % and 60 %.

Results from the EOF analysis reveals distinct differences between the sampling years, most prevalent is the opposing regime from 2018 to 2019. During 2018, $PC1_{\delta^{18}O}$ and $PC1_{dxs}$ have an inverse correlation in the spatial dimension ($r=-0.6$),

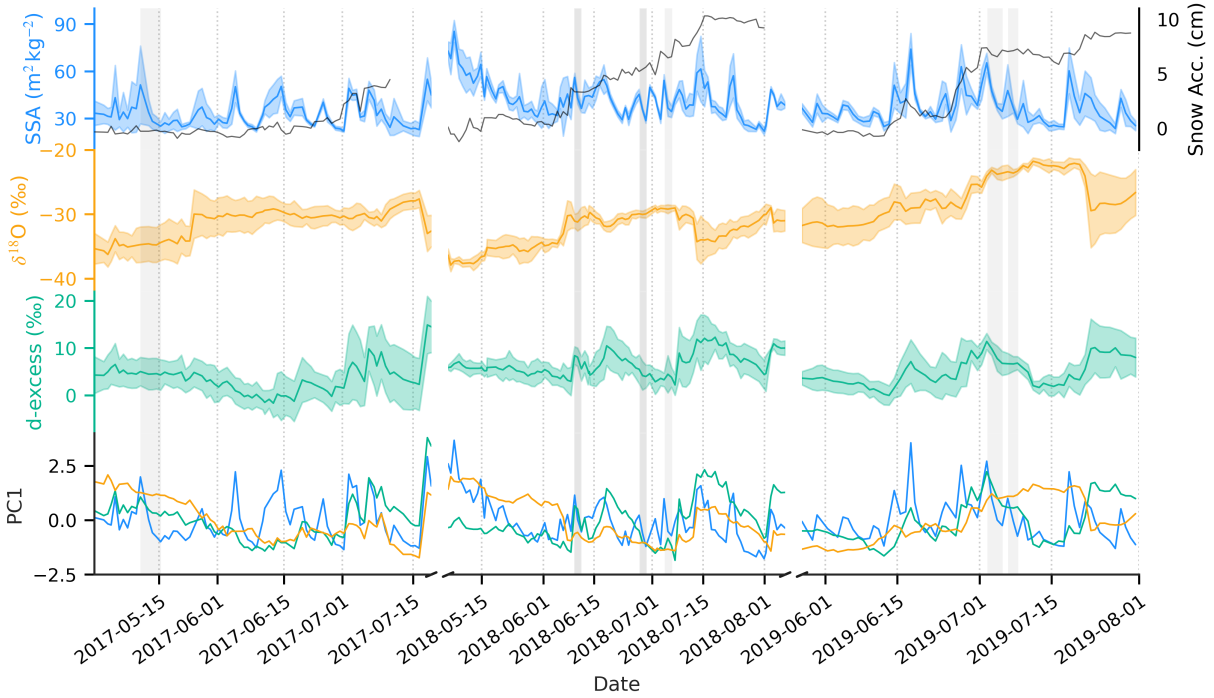

Figure 3. ~~*SSA Timeseries 2017, 2018 and 2019*~~Time-series of SSA ~~time-series between May and August for a~~(blue)~~2017~~, ~~b~~d18O (orange)~~2018~~ , *d*-excess (green) and ~~e~~the first principal components (PC1) ~~2019. Faded lines represent~~ of each variable in the ~~10 individual samples from~~ lower panel. Bands in the ~~90 m~~ upper three panels show spatial standard deviation between the 10 sampling ~~transect, while~~ sites. The secondary y-axis in the ~~bold line~~ top panel shows the ~~daily mean values~~average snow accumulation. ~~Gaps in the timeseries represent missing data. Grey~~ The grey bars ~~highlight~~ indicate the ~~periods of decrease in~~ SSA ~~defined by the threshold algorithm for each year. Six decrease~~ decay events~~are observed in 2017 and 2019, while nine are observed in 2018. Decrease events are interpreted as rapid grain growth due to snow metamorphism, and stars indicating days with precipitation~~.

and a significant positive correlation between $PC1_{\delta^{18}O}$ and $PC1_{dSSA}$ in the temporal dimension ($p<0.05$, $r=0.5$) (Fig. A2 and Fig. A3). In contrast, data from 2019 are 92characterised by significant positive correlations between $PC1_{SSA}$ and of $PC1_{dxs}$ in both the spatial (p m^2<kg^{-1} and 820.05, r m^2=kg^{-1} respectively, while during 0.75) and temporal dimensions ($r=0.3$, $p>0.05$), while no relationship is observed between $PC1_{\delta^{18}O}$ and $PC1_{dxs}$. During 2017there are only two instances of daily mean SSA being above 60, there is a weak positive correlation the temporal component of $PC1_{SSA}$ and $PC1_{dxs}$ (p m^2<kg^{-1} .0.05, $r=0.3$), and the temporal $PC1_{\delta^{18}O}$ and $PC1_{dxs}$ ($p<0.05$, $r=0.4$). There is an apparent shift after July 15th where $PC1_{dxs}$ transitions from co-varying with $PC1_{\delta^{18}O}$ to co-varying with $PC1_{SSA}$. Figure A2 and Fig. A3 in the supplement illustrate the spatial and temporal components of the EOF results.

A visual inspection of the decay events in Fig. **??** indicates

3.1 SSA decay events

3.1.1 Observations

In agreement with Eq. (1), we observe a relationship between initial SSA and subsequent magnitude of decrease . To test whether the mechanisms of decay are consistent throughout events when evaluating the SSA decay events (Fig 3). From the years 2017, 2018 and 2019 a total of 21 events are identified that fulfill the SSA decay criteria (as defined in Section 2.5.1). These events are named E1, observed SSA decays are analysed to construct an empirical model. E2 etc (Table A).

3.2 EastGRIP SSA decay model

Continuous SSA measurements allow for the construction of an empirical model to describe SSA decay at EastGRIP through time while exposed to surface processes. All samples of defined SSA decrease events Prior to analysis, we assess the meteorological conditions and field observations to remove SSA decay events with potentially perturbed surface snow. This includes all events coinciding with observations of ground fog, snowdrift, and snowfall, and events where the wind-speed exceeds the thresholds defined in Section 3.1 are used to quantify surface snow metamorphism. For all eventswith mean temperature above -252.5.1. Out of 21 events captured by the SSA decay event threshold, 15 are influenced by either snowdrift, snowfall, or ground fog according to field diary observations, or high wind-speeds (maximum wind-speed >°C, the mean SSA of the final day is around 307 $m\,s^{-1}$). Of the remaining 6 events, two are in the low-wind category (E10 and E11 = 5.1 $m\,s^{-1}$), and 4 in the moderate-wind category. Both E10 and E11 had consistent clear sky conditions. Note that E11 was preceded by significant ground fog, not snowfall, indicating that the peak value of 46 $m^2\,kg^{-1}$ (referred to as the background decay state). A relationship is observed between the was likely the result of surface hoar, and thus, rapid SSA decay follows an SSA peak not caused by precipitation.

fc8d62 8da0cb

The rate of SSA decay is closely linked to the SSA value at the start of each event (initial SSA vs. magnitude of decrease strongly influenced by the initial SSA during the decay period $r^2 = 0.4$) (Fig. 4), suggesting showing that the rate of change is proportional to the absolute value, as described by an exponential decay law ($r=-0.71$ and $r=-0.91$ for low- and moderate-wind events respectively). The mean air temperature for all SSA decay events was between -17.3 °C and -7 °C. The first day of

each event is characterised by the largest change in SSA, followed by a decrease in magnitude over the subsequent days, with negligible change in SSA below 22 $m^2\,kg^{-1}$.

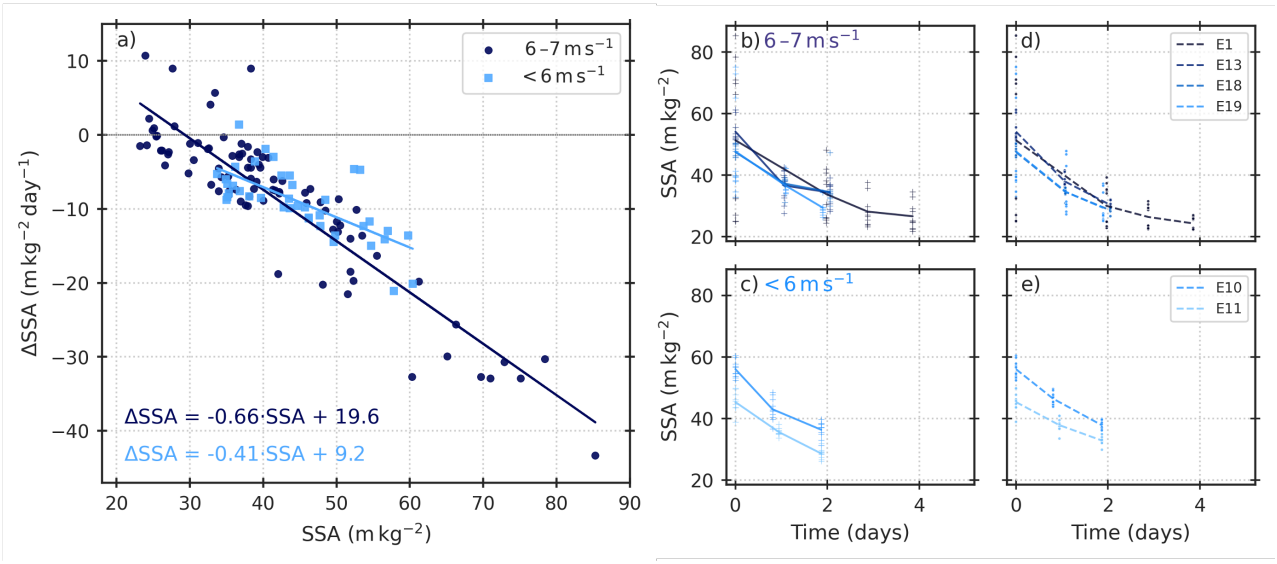

Figure 4. Linear regressions for change in SSA against the SSA for the low-wind (light-blue) and moderate-wind (dark-blue) SSA decay events (a) considering all individual samples. The observed SSA decays are shown for the moderate-wind events (b), and the low wind events (c), followed by the modelled SSA decays for the respective events in d) and c). The legend in d) and e) corresponds to SSA decay event number in Table A

3.1.1 Model

SSA decay rate is quantified by plotting the rate of change in SSA per day against the absolute SSA value for all 10 sampling sites for ~~all~~ low- and moderate-wind events (Fig. 4a). We observe a linear relationship between the ~~rate of~~ change in SSA ~~per day~~ from one day to the next (ΔSSA) and SSA. ~~Outliers are measurements from days with mean air temperature below -25 °C as highlighted in Fig. 4a. This observation is in agreement with theoretical understanding of snow crystal formation transitioning from dendrites to columns at approximately -22 °C (Domine et al., 2008). We therefore define the SSA decay model for a temperature range between -25 °C and 0 °C and daily mean wind speeds below 6 m s^{-1} based on hourly averaged values.~~

~~Constructing the~~ The SSA decay model for EastGRIP is ~~based on~~ constructed using the differential equation for the linear relationship between ΔSSA and absolute SSA~~which is defined as Eq. (??).~~ . Solving the differential with respect to time (t), produces the SSA decay model defined as Eq. (5), which follows the equation structure ~~from~~ of Eq. (1).

$$\frac{dSSA}{dt}SSA(t) = -0.54(SSA_0 - 22) \cdot e^{-\alpha \cdot t} + 14.6922 \tag{5}$$

$SSA(t) = (SSA_0 - 26.8)\, e^{-0.54t} + 26.8$

Where SSA(t) is the SSA measurement at a given time in days since the first measurement (initial SSA), SSA_0 is the initial SSA value, and -0.54 $m^2\,kg^{-1}\,day^{-1}$ α is the decay rate(α), as defined by the slope of Eq. (**??**). To account for a non-zero decay constant , the value 26.8, and a decay constant of 22 $m^2\,kg^{-1}$ is defined by for both equations by the minimum SSA value where the derivative of SSA is equal to 0 $m^2\,kg^{-1}$. The decay rate, determined by the value of x when the linear regression crosses the y-axis (Fig. 4a). The SSA decay model describes rapid decrease in SSA based on empirical data from EastGRIP, Greenland.

3.1.2 Model evaluation

*Decay Model Construction and Predictions*All samples for all events are included in plot a) showing the relationship between the rate of change in SSA per day (ΔSSA day^{-1}) against the daily absolute values. Points are coloured by the daily mean surface temperature. The linear regression is based on values for surface temperatures between -25 °C and 0 °C, and daily mean wind speeds below 6 $m\,s^{-1}$. b) shows a comparison between the model predicted SSA values using Eq. (5), against the SSA observations. The marker colour represents the day of the events (DOE). Marker style represents the sampling year to assess inter-annual variability for 2017 (o), 2018 (x) and 2019 (□). c), d) and e) show all included events in full-line and f), g) and h) show the model predictions as the dashed line. E1-E21 refers to events as listed in Table A. Missing data day-1 E1.

Model performance is tested by comparing daily predicted decrease to the 10 daily observations. Model-data residuals for daily data are normally distributed, suggesting no systematic errors in model predictions. Figure 4 shows the construction of the model (slope of the linear regressions in Fig. 4, a-b) and prediction of SSA decay (Fig.4,f-h). Note that events are here named E1, E2... consistent with Fig. **??** and also listed in Table A.

There is a minor tendency for the model to underestimate the SSA decrease and thus overestimate the predicted values of SSA as seen in Fig. 4b. Model limitations are most evident during the first day, as seen in Fig. 4, where the modelled decay consistently underestimates the magnitude of decrease . The model has limited ability to predict observations below in the lower range of SSA observations as seen in Fig. 4f, g and h, where the modelled and observed values are compared for each event.

Following our definition in Section 3.1 the events have an extent of 2-5 days. To assess model performance in predicting magnitude of SSA decrease for events of different time periods, we compare the predicted versus measured SSA. For rapid events lasting 2-days the model tends to underestimate the rate of decrease. This is most apparent on Day 1 (24h after peak) for 2017 and 2018, while for 2019, Day 1 SSA is accurately predicted , with residuals increasing on Day 2. In comparison, events lasting 5-days show an underestimation for 2017 with negligible daily change in residuals, while the model overestimates the decay rate of E14 in 2018. However, field documentation suggests intermittent snow fall during Day 2 of E14, causing increase in SSA. Consideration for environmental context is explored in Section 2.5.1. E16 is characterised by the highest initial SSA values, and the largest residuals, suggesting the model is limited at very high initial SSA values.

The model requires only initial SSA as a parameter and predicts SSA decrease at EastGRIP within the defined conditions with an averaged root mean squared error (RMSE) of 5.6is higher for moderate-wind SSA decay events (-0.66 $m^2\,kg^{-1}$ when considering all sample sites individually. The model predicts SSA decay over 2-5 day periods (r^2 = 0.89), with the highest

~~RMSE of 6.17~~ day^{-1}) than for low-wind SSA decay events (-0.41 m^2 kg^{-1} ~~for 2019 compared to 4.97~~ day^{-1}). Within the temperature range of low- and moderate-wind SSA decay events from this study, there is no observable temperature dependence of the SSA decay rate. However, such a temperature dependence is clear in events which were excluded due to potential surface perturbations, where there is a decrease in decay rate and increase in the background SSA value with low temperatures (Fig. A4). Our results indicate a slower rate of decay under decreased wind-speed conditions.

3.1.2 Model performance

Table 2. RMSE values for model evaluation. This Study uses the respective α for the low- and moderate-wind events for daily (mean) and individual samples. FZ06 parameters τ and n are defined from the look-up table in Flanner and Zender (2006). T07 uses the mean surface temperature for each event as an input parameter.

	Low-wind		Moderate-wind	
	Mean $m^2\,kg^{-1}$	Individual $m^2\,kg^{-1}$	Mean $m^2\,kg^{-1}$	Individual $m^2\,kg^{-1}$
This Study	2.48	3.50	2.60	4.28
FZ06	6.46	6.90	7.90	9.52
T07	5.63	6.10	5.27	6.49

Model performance is tested by comparing daily predicted decrease to the 10 daily observations, and by comparing model predictions from this study to those from Flanner and Zender (2006) hereafter referred to as FZ06, and the model defined by Taillandier et al. (2007), hereafter T07, as defined in Section 2.5.2. Residuals between our model and the observations are normally distributed, suggesting no systematic errors in model predictions. The root mean squared error (RMSE) between our model predictions and observed mean SSA is 2.48 m^2 kg^{-1} ~~and 4.72~~ and 2.60 m^2 kg^{-1} for ~~2017 and 2018 respectively. The model adequately predicts rapid SSA decay at EastGRIP within the temperature range, while for colder temperatures,~~ the ~~decay rate is the same but the intercept is significantly higher (Fig. 4a). Overall, for all included events during the three sampling years, behaviour of SSA decay is clearly captured by the model (Fig. 4c, d and e). Exploring temperature conditions alone we find that the model performs well when daily mean surface temperatures are between -25 °C and 0 °C.~~ low-wind and moderate-wind SSA decay events respectively.

3.1.3 ~~Environmental conditions during SSA decay events~~

~~Intuitively, environmental conditions would be considered to play a role for surface snow metamorphism and the rate of SSA decay . To explore this, hourly weather measurements from the PROMICE AWS and field report weather observations are analysed to provide environmental context to SSA decay events. Weather station data shows no systematic influence of basic weather variables, relative humidity, surface temperature and wind speed on the model-data residuals, with linear regressions resulting in $r^2 < 0.1$ for all variables. An overview of event conditions using field observations are~~ Parameter values for τ

and n in FZ06 are defined for each event based on mean density, surface temperature and temperature gradient using the extensive look-up table referenced in Flanner and Zender (2006). FZ06 consistently overestimates the SSA decay rate, with residuals increasing throughout the events (See Fig. A5). T07 is able to accurately predict the moderate-wind events, with largest errors associated with E1, the event featuring the lowest temperatures and highest wind-speeds. which has relatively lowest temperatures and highest wind-speeds. However, for low-wind events T07 consistently underestimates the SSA decay rate. RMSE values presented in Table ~~A. Temperatures below -25°C are characterised by the same slope defined by the model ($-0.54\,m^2\,kg^{-1}\,day^{-1}$), but with a significantly higher intercept of $29\,m\,s^{-1}\,day^{-1}$ compared to $14.7\,m\,s^{-1}\,day^{-1}$ for temperatures above -25 °C. Significant wind drift is expected when hourly mean wind speed exceeds $6\,m\,s^{-1}$, which happens during 144 days out of the total 258 sampling days from 2017, 2018 and 2019. Results indicate weather has no systematic influence on SSA decay during the first 2-5 days exposed at the surface, and that conditions vary for each event. The model is able to predict all defined decay events between -25 °C and 0 °C, indicating mechanisms of decay are the same. Daily mean values are more accurately predicted by the SSA decay model than individual sample sites due to snow surface variability. In-homogeneous surface snow is especially important to consider for isotopic composition, because there is potential for samples to contain snow from different precipitation and/or deposition events.~~ 2 indicate that the model from this study predicts decay with the least error, for both wind-speed categories.

3.2 Isotopic change during SSA decay events

3.2.1 Low- and moderate-wind event analysis

3.2.2 ~~Surface snow spatial variability~~

~~The characterization of the SSA decays provide a basis to explore how snow metamorphism of surface snow plays a role for the alteration of isotopic compositionof Greenland snow after deposition. A recent study at EastGRIP has shown the significant in-homogeneity in surface snow due to post-depositional reworking of the snow (Zuhr et al., 2021). The focus for this manuscript is to identify signal coherence between physical properties and isotopic composition of surface snow subject to precipitation/deposition and post-depositional processes. Autocorrelation analysis shows that isotopic composition values are spatially decorrelated after 10 m ($r^2 < 0.3$ after 10 m). Therefore, to avoid attenuation of isotopic signal, each sample is treated as independent. Isotopic composition is measured from each SSA sample containing snow from the top 2.5 cm of the snow surface, potentially containing snowdeposition layers from multiple precipitation events. Surface heterogeneity is considered by using Empirical Orthogonal Function (EOF) analysis to determine the dominant mode of variance for each sampling year. Figure **??** shows timeseries of $\delta^{18}O$ (a), d-excess (b) and SSA (c) with faded lines showing each sample site. The first principal components (PC1) of $\delta^{18}O$, d-excess and SSA are presented in Fig. **??**d. All parameters continuously change throughout the field seasons of 2017, 2018 and~~ EOF analysis in Section 3.0.1 indicates a relationship between SSA and isotopic composition, most pronounced in 2019. ~~Isotopic composition measurements (Fig. **??**a, b) have larger spatial variability than~~ With the understanding that decreasing SSA for low- and moderate-wind events is the result of snow metamorphism of an

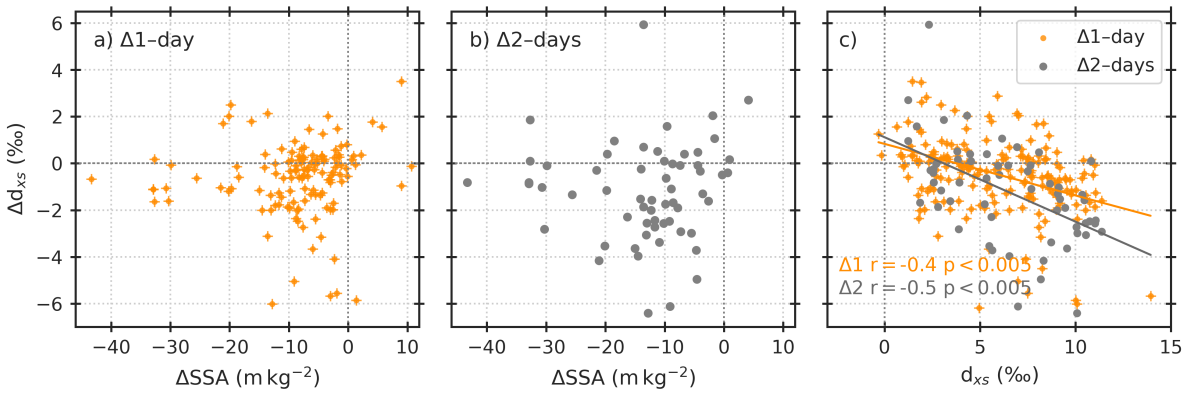

Figure 5. ~~*Timeseries of snow isotopes and SSA*~~Timeseries of δ^{18}O ~~(a)~~Isotopic changes during all the analysed events are shown, ~~d-excess~~ with each point indicating a specific sampling site. The daily change in *d*-excess (~~b~~d_{xs}) and SSA ~~(c~~is presented in a)~~for 2017~~, ~~2018~~ change in *d*-excess and ~~2019 sampling seasons. d) shows~~ SSA over the ~~principle components~~ first 2-days of each ~~parameter with colors corresponding to the color used to show absolute values. The black vertical lines indicate a break~~ event is shown in ~~the x-axis. Each faded line represents individual sample site values~~b), and the ~~thick line is~~ respective changes in *d*-excess are plotted against the ~~daily mean. Grey shaded regions indicate periods of high spatial variability~~ absolute *d*-excess values in ~~isotopic composition~~c). Linear regressions are included for daily change (orange) and 2-day change (grey).

unperturbed snow surface, we can now document concurrent isotopic changes in the snow. For both low- and moderate-wind events, rate of change in *d*-excess is plotted against the rate of change in SSA (Fig. **??**~~c).~~

~~Inter-annual variability is observed in δ^{18}O, with seasonal mean values of -31.6‰5), -32.7‰ and -27.3‰ for 2017, 2018 and 2019 respectively (Fig. **??**a). Note that the 2019 field season started approximately 15 days later than 2017 and 2018, resulting in a bias towards mid-summer conditions. Throughout the season δ^{18}O follows a gradual increasing trend from May to August. Some cases of abrupt decreases (-10‰) are observed in the late summer, for example at July 12th in 2018 and July 25th in 2019. No clear seasonal trend is observed in d-excess (Fig. **??**b) but with periods of gradual decreases. Total daily spread in δ^{18}O and d-excess is ~15‰.~~

~~During 2017, 2018 and 2019 SSA has one dominant mode of variance (PC1) explaining 61%, 77% and 72% of the total variance in~~ after the first and second day of each event. We here include analysis of the ~~respective datasets. PC1 of δ^{18}O explains 69%, 83% and 75% of the total variance for the respective years. While PC1 of d-excess explains 47%, 51% and 60% for 2017~~change in *d*-excess after the second day (referred to as a 2-day change), ~~2018 and 2019 respectively. PC1 of δ^{18}O and d-excess show strong coherence from May to early June during 2017 and 2018, while for the second half of the season, and throughout 2019, PC1 of d-excess corresponds to PC1 of SSA (Fig. **??**d).~~

~~Surface variability due to post-depositional reworking of the snow is shown by a wide spread in SSA values during a given day. Time periods with low spatial variability indicate largely homogeneous snow cover over the transect, shown in Fig. **??** as shaded regions. High variability is defined by periods where the 5-day running-mean of spatial variance in δ^{18}O is greater than~~

one standard deviation. During periods of low spatial variability in isotopic composition, there is greater coherence between PC1 of SSA and PC1 of d-excess, due to a reduction of noise in the dataset. PC1 of SSA and d-excess show a coherence during 2018 and 2019 seasons, while the signal is less clear during 2017 (Fig. **??**b). However, the reduced signal coherence is concurrent with high spatial variability in isotopic composition.

A clear relationship between PC1 of SSA and PC1 of d-excess is observed when there is a relatively homogeneous snow layer over the sampling transect, defined by low spatial variance in δ^{18}Opresented in Table 3 for each low- and moderate-wind events.

3.2.2 Isotopic change during decay events

*Relationship between SSA and d-excess after the second day of each event*The relationship between the rate of change in SSA (ΔSSA $2days^{-1}$) and d-excess (Δd-excess $2days^{-1}$) over a 2-day period for a) individual samples for events presented in Table 3 for 2017 (o), 2018, (x) and 2019 (□), b) the same values colour coded by initial d-excess from each event. c) shows the relationship between change in d-excess after 2-days plotted against the initial d-excess value, with the linear regression line in black.

Using all 10 sample sites as independent values, the behaviour of isotopes during defined SSA decay events is analysed. To determine the isotopic change in the surface snow during rapid SSAdecays, the rate of change in d-excess is plotted against the rate of change in SSA (Fig. 5). The change in SSA over a 2-day period is used. The daily mean change over the first 48h of each event is presented in Table 3.

*Table of isotopic change for decay events*Behaviour

Table 3. Table of snow parameters during isotopic change for decay eventsare defined. The initialMean values on day-0 and day-2 of each event, 2-day and percentage change over a this 2-day period are presented for δ^{18}O, d-excess *d*-excess and SSA. All Low-wind events used for the decay model are presented here, thus only the low-temperature event E7 (<-30 °Cbold text) is removedand moderate-wind events are presented.

E2 -30.29 -30.15 0.5% 0.9 -0.3 -133% 50.1 28.2 -43.7% **E3** -29.55 -30.07 -1.8% -0.2 -0.6 -200% 50.4 31.1 -38.3% **E4** -30.27 -30.15 0.4% 1.4 -0.2 -11

E14 -33.89 -34.26 -1.1% 11.5 12.3 7.0% 53.2 37.4 -29.7% **E15** -32.35 -

E20 -22.27 -2

~~In all events , the isotopic composition is observed to change, with~~ Both δ^{18}O ~~increasing after~~ and *d*-excess change from the initial value (day-0) in all events, with the percentage change in *d*-excess being the same order of magnitude as for SSA, and an order of magnitude higher than that of δ^{18}O. Three out of six events are characterised by increasing δ^{18}O and decreasing *d*-excess after 2-days~~but mostly limited to 1±1‰ mean increase, with the exception of E17~~. E1, E13 and ~~E21 in 2019 (See Table 3)~~ E19 deviate from this pattern. E13 and E19 both correspond to total increase in δ^{18}O and *d*-excess, whereas E11 is characterised by a slight decrease in δ^{18}O and decrease in *d*-excess (Table 3). ~~E17 is characterised by significant ground fog and snowfall during the event, while E21 has negative LHF (net-deposition)measured from the eddy-covariance system over the event. The percentage change~~ The Δd-excess over 1-day indicates a slight negative skew around a mean of ~~d-excess is an order of magnitude higher than $\delta^{18}O$ - expected due to the definition of d-excess - and similar to SSA, with 14 out of 19 events showing a decrease in d-excess during the first 2-days of each event. Further analysis looks specifically at the relationship between d-excess and SSA given the coherence observed between their PCs, and the significant change observed in Table 3.~~

~~SSA decreases by between 30~~-0.3 ~~% and 53~~‰. 4 of 6 events (61% of all sample sites) experience a decrease in *d*-excess by day-2. The mean is shifted to -1.2 ~~% during the first 2-days, the largest change corresponding to the highest initial SSA value of 74~~‰ over a 2-day period with decreases in *d*-excess documented in 45 out of the 60 samples (75%) during precipitation-free periods with minimal surface perturbation. Initial *d*-excess is observed to have a significant influence on the magnitude of *d*-excess decrease over the defined period (Fig. 5c), with high initial *d*-excess corresponding to the largest decreases in *d*-excess.

3.2.2 Low-wind event analysis

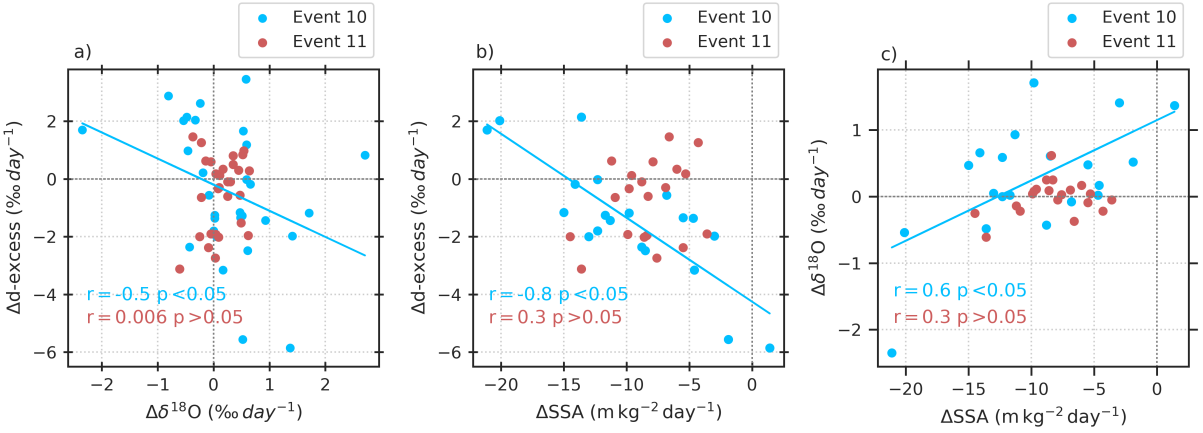

Figure 6. Isotopic change analysis for low-wind events, E10 and E11. Panel a) shows daily change in *d*-excess against change in δ^{18}O for E10 and E11, b) shows change in *d*-excess against change in SSA, and c) shows change in δ^{18}O and change in SSA. The r- and p-value for each regression are indicating in the corresponding colours. Only significant linear regressions are indicated with a line.

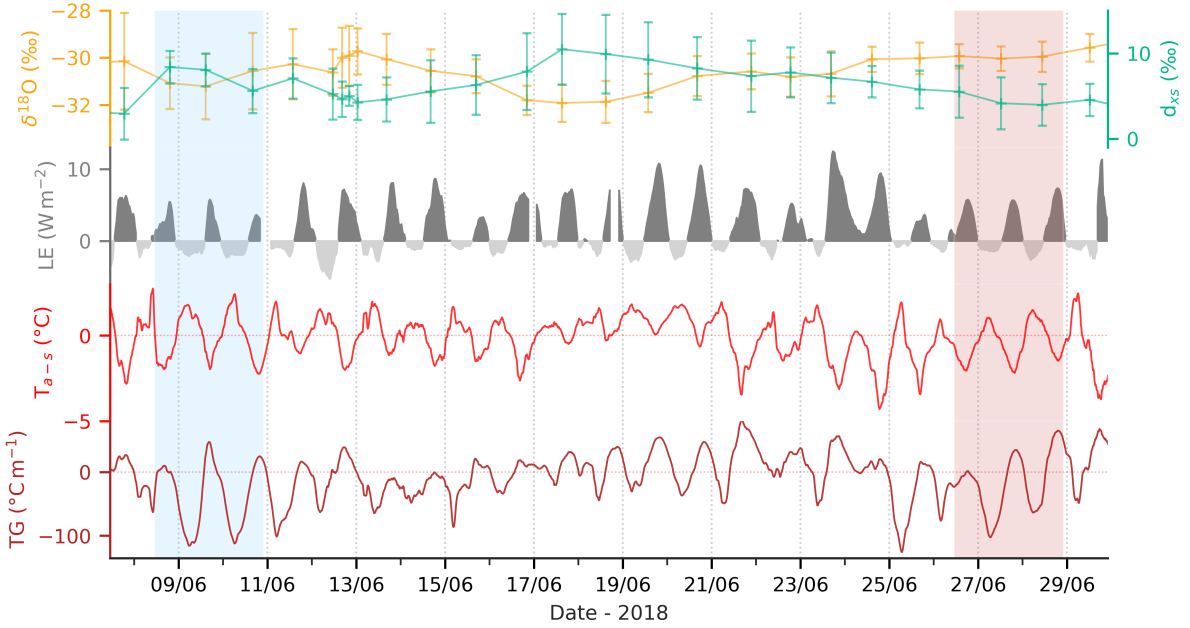

Figure 7. LE and temperature gradients for low-wind events. Latent heat flux (LE) (grey), air-surface temperature gradient (TG) (red) and surface-10 cm subsurface TG (red) during June 2018. E10 (blue) and E11 (red) are highlighted. Dark grey shading in LE indicates sublimation and light grey shows deposition.

The following section focuses on latent heat fluxes and near-surface temperature gradients corresponding to isotopic change during low-wind events only. This is to ensure that surface layer we are analysing is constant throughout the event to avoid inaccurate interpretation of isotopic change. As mentioned in Section 3.1, ground fog preceded the SSA peak in E11, concurrent with negligible accumulation recorded. In contrast, almost 1 ~~$m^2\,kg^{-1}$ as defined by the decay model. Using a significance level of 0.01,~~ cm of snow was accumulated during the day prior to E10, corresponding to observation of snowfall.

Figure 6 shows the relationship between ~~change in d-excess after the second day of each event~~ the daily change in isotopic composition for E10 and E11 (~~Δd-excess) and change in SSA over the same time period~~ *d*-excess and $\Delta\delta^{18}O$) and SSA (ΔSSA)~~is assessed. Events presented in Table 3 are shown in Fig. ??a. 72~~. During E10, significant inverse correlations are observed between $\Delta\delta^{18}O$ and Δd-excess, and between ΔSSA and Δd-excess (r~~% of decreases in SSA correspond to decrease in d-excess when treating each sample as an independent value. All large decreases in SSA correspond to high SSA values, as the model describes. Increases in d-excess are observed at 12 samples sites, 6 of which are during 2017 and all correspond to initial d-excess values~~ = -0.5, r=-0.8), while $\Delta\delta^{18}O$ and ΔSSA are positively correlated (r=0.6). In contrast, no significant relationship is observed between the Δ-parameters during E11, where there is negligible change in surface snow $\delta^{18}O$ (<~~5‰ (Fig. ??b). Thus suggests either low d-excess of deposited snow, or old snow that has been re-exposed. In addition, initial d-excess is observed to significantly influence that magnitude of d-excess change over the subsequent 48h of rapid SSA decay~~

(Fig. ??a and b). The largest changes in d-excess corresponds to high initial d-excess values. Moreover, increases in d-excess during rapid SSA decay follow very low initial d-excess values. In summary, in 720.7 % (78 out of 108 samples)of cases decreases in SSA correspond to a decrease in d-excess of the snow sample during the first 2-days. Moreover, the magnitude of change in d-excess during rapid SSA decay shows a weak but significant dependence on the initial d-excess signal. ‰).

Significance of change in SSA and d-excess during events is tested by comparing the difference between the means of daily changes for event and non-event periods using a t-test with 0.01 significance level. Background variability in d-excess is 0.1±2.5The direction of vapour fluxes are inferred using temperature gradients determined from air, surface and subsurface (10‰ for non-event periods, compared to -0.4±2cm depth) temperature data, and LE, measured as an upwards flux. Net-sublimation is observed during both E10 and E11, with a total sum of 33.9‰ for events alone. Similarly for SSA, non-events daily change is 0.04W m$^{2-2}$ and 55.8 kg^{-1} compared to -7.7W m$^{2-2}$ for the respective events. LE is inversely related to the temperature gradient (TG) between the air and the surface, with strong sublimation (>kg^{-1} for events. SSA decay events exhibit significant difference in distribution to non-event daily changes ($p < 0.01$, $t = 4.0070$, $df = 1715$, Std. Err. = 0.125) . Moreover, changes in d-excess during events are double the magnitude of background variability with a consistently negative sign for all years, supporting evidence that d-excess of recently deposited snow has a 7210 % chance of decreasing during surface snow metamorphism (SSA decay) during the first two days, according to our data. W m^{-2}), corresponding to a negative TG of 2.5°C between the air and surface on June 10th. A concurrent upwards vapour flux is observed between the subsurface and surface, most apparent on June 11th (Day-2 of E10).

Analysis shows that rapid SSA decay events correspond to decreases in d-excess over a 2-day period in 72Negative LE up to -4 % of the samples. Results from EOF analysis during periods of low spatial variance in isotopic composition over the sampling transect reveals a coherence between the dominant mode of variance of SSA and d-excess, suggesting that processes driving change in SSA also influence d-excess. W m^{-1} are documented each night corresponding to the transition from a negative to positive TG between the air and surface. Net-deposition was recorded between sampling on 9th June at 15:18 UTC and 10th June 10:40 UTC (first day of E10) corresponding to a decrease in δ^{18}O and *d*-excess. The subsequent day, characterised by net sublimation, had a large increase in δ^{18}O and a larger decrease in *d*-excess. Contrary to E10, E11 is characterised by a large decrease in *d*-excess and a small decrease in δ^{18}O, both concurrent with net-sublimation and strong negative surface-subsurface TG. The air-surface TG during E11 has a lower mean and reduced diurnal amplitude than E10 facilitating sublimation for a longer period.

4 Discussion

Continuous daily SSA measurements at EastGRIP have enabled during the summer season of 2017, 2018 and 2019 have allowed for quantification of variations in snow physical properties due to precipitation deposition and snow metamorphismduring summer. Understanding the relationship between rapid decreases in SSA and corresponding change in isotopic composition require clearly defined events and environmental context. Using a multi-day SSA decrease threshold, 21 events are defined from the summer field seasons of 2017, 2018 and 2019. All events are characterised by a peak and subsequent decay in SSA ,

the rate of which is proportional to the initial SSA value. SSA decay in precipitation free periods is driven by sublimation and vapour diffusion which is expected to influence the snow isotopic composition (Ebner et al., 2017; Hughes et al., 2021). set of criteria, six SSA decay events during precipitation-free periods are defined and used to construct an empirical decay model with the decay rate tuned for low and moderate wind-speeds. We firstly discuss the behaviour of SSA decay at EastGRIP and compare to existing models. The isotopic change associated with low-wind SSA decay events is then considered, in the context of sublimation, interstitial diffusion and wind effects (Ebner et al., 2017; Hughes et al., 2021). Results from EOF analysis are used in combination with the isotopic change during SSA decay.

4.1 Decay model developments

4.1 SSA decay at EastGRIP

In this study, we present an empirical SSA decay model for surface snow of polar ice sheets based on continuous daily SSA measurements. The model describes SSA decay under natural summer conditions on the ice sheet. The findings from this study agree with previous studies, that SSA decayis most accurately Events of rapid SSA decay at EastGRIP are best described by an exponential function (Cabanes et al., 2002), and indicates that the crystal structure of a new snow layer is a key driver of decay rate within the defined conditions over 2-5 day periods.

Comparison with weather station data showed that the SSA decay rate during events had no systematic influence from weather variables (wind speed, temperature and relative humidity) decay function, in agreement with observations from Cabanes et al. (2003). No cold events (< -20 °C) are captured within the event criteria, potentially indicating 1) a need for warmer temperatures to induce such change in SSA over the time-period, or 2) that the local synopticity favours precipitation coincident with low temperature and high winds during the summer. Within this framework, the events captured by the threshold with mean temperatures below -20 °C are likely capturing wind-erosion, exposing sub-surface snow with lower SSA. The only exception is for temperatures outside the set range for the model. Surface temperatures below -25 °C were characterised by a significantly higher background SSA(defined as the mean SSA value of the final day of decay events) (Fig. 4), indicating high background SSA due to reduced snow metamorphism in colder conditions. This observation is supported by theory and observation that sublimation and deposition are thermally activated processes (Cabanes et al., 2003). Taillandier et al. (2007) (T07) developed an SSA decay model with a surface temperature parameter in addition to initial SSA which is able to capture the behaviour of decay during the cold event, E7, at EastGRIP suggesting temperature is important to consider when predicting SSA outside the defined temperature range. However, the influence of temperature on SSA decay rate within the defined temperature range is negligible. Model-observation comparisons show equal performance for the SSA

The narrow temperature range of SSA decay events does not facilitate a conclusive definition of a temperature-dependent decay rate (Cabanes et al., 2003; Legagneux et al., 2003; Flanner and Zender, 2006; Taillandier et al., 2007). We instead assess the influence of wind-speed on the SSA decay rate and observe a more rapid SSA decay with increased wind-speed, which can be explained by increased ventilation of saturated pore air acting as a catalyst for snow metamorphism (Cabanes et al., 2003; Flanner and Ze

.

Unsurprisingly, given the parameters are fit to the data, the model defined in the study predicts SSA decay for the low- and moderate-wind events with the lowest RMSE. The decay model from ~~this study ($r^2 = 0.89$) compared to~~ Taillandier et al. (2007) (T07~~temperature gradient metamorphism model ($r^2 = 0.9$) .~~

~~The top 1~~) performed well. performed well for the moderate-wind events, but underestimated the rate of decay for the low-wind events. T07 was defined based on the SSA decay of fresh snow with densities below 180~~cm of the 2.5~~kg~~cm SSA sample is measured by the Ice Cube device, and thus, is most likely to capture the precipitation signal (Gallet et al., 2009; Klein, 2014) . Directly after precipitation, isothermal snow metamorphism is expected to be dominant due to to high surface curvature of fresh snow crystals (Colbeck, 1980). Alternative SSA decay models are proposed by Taillandier et al. (2007) to describe snow metamorphism under temperature gradient (temperature driven recrystallisation) and isothermal (curvature driven recrystallisation) metamorphism, with the surface temperature and initial SSA being variable parameters. However, we find that all events are most accurately predicted using the temperature gradient decay equation, which accounts for the very low surface temperature observed in E7. The similarity in prediction for ~~-25~~m^{-3} (Taillandier et al., 2007), compared to a mean density of 266~~°C to 0~~kg~~°C suggests the EastGRIP SSA decays are not only driven by crystal curvature but by temperature gradient vapour diffusion as well.~~

~~The influence of snow metamorphism after precipitation during winter is expected to be reduced due to low temperatures and negligible temperature gradients during polar night. Based on this~~m^{-3} for all low- and moderate-wind events in this study. The tendency for T07 to underestimate the SSA decay seems counter-intuitive given the possibility of aged snow in our study, which would plausibly be expected to experience SSA decay at a slower rate that fresh snow (Domine et al., 2007). In contrast, the model ~~is only recommended to use for polar ice sheet summer conditions only. Within the defined conditions, the SSA decay model is a simple empirical model to describe SSA decay in the accumulation regionsof the Greenland Ice Sheet, with dependence on the initial SSA alone~~from Flanner and Zender (2006) (FZ06) consistently overestimates the observed SSA decay rate, most pronounced in E10 and E18. The original parameter values τ and n were tuned to data from alpine regions, potentially explaining the poor fit.

4.2 ~~Decay model applications~~

~~Conditions for the model are expected to be applicable over the Greenland Ice Sheet interior under mean summer conditions . The model predicts decay events at EastGRIP with a r^2 of 0.89, compared to observation, within defined conditions. SSA estimates from satellites have previously been compared to ground observations and show a strong correlation between daily mean SSA and satellite retrieved SSA at EastGRIP(Kokhanovsky et al., 2019). The SSA decay model has the potential to predict SSA decay over the entire accumulation zone of the Greenland Ice Sheet using satellite data, the model can be evaluated for different sites to document the spatial variability in SSA over the entire ice sheet, and describe the summer SSA decay. This has additional benefits for quantification of surface mass balance and surface energy budget due to the relationship between snow microstructure and surface albedo.~~ The simple empirical model presented here is limited to conditions at EastGRIP within a narrow temperature range and therefore is likely to be unsuitable for sites with different conditions. However, large errors

when using the models from the literature indicate that the low-latitude tuning is not optimal for predicting surface snow SSA decay at EastGRIP.

4.2 Isotopic change during SSA decay events

4.2.1 Low-wind events

4.3 ~~Rapid SSA decay and d-excess~~

Three key mechanisms are expected to drive the rapid SSA decays, 1) large grains growing at the expense of small grains (Legagneux et al., 2004; Flanner and Zender, 2006), 2) diffusion of interstitial water vapour (Colbeck, 1983; Ebner et al., 2017; Touzeau et , 3) sublimation reducing the dendricity of snow grains which is intensified by wind ventilating the saturated pore air, known as 'wind-pumping' (Neumann and Waddington, 2004). The dominant mechanisms can theoretically be identified by a combination of the change in isotopic composition - indicating the fractionation effect - and the LE and temperature gradient data to determine the direction of flux.

~~In this study, processes driving snow metamorphism are documented to influence isotopic composition of the snow after precipitation, supporting experimental observations and theoretical understanding (Ebner et al., 2017; Wahl et al., 2021; Hughes et al., 202 . Results from this study suggest that surface snow metamorphism following precipitation events corresponds to change in isotopic composition, most clearly observed in d-excess (Table 3). Based on our results, rapid decreases in SSA correspond to decreases in d-excess of a new snow layer in 72 % of cases during the first 2-days of rapid SSA decay .~~

~~Using the eddy-covariance latent heat flux measurements, we observed net sublimation during all decay events (with the exception of E21)used for isotopic analysis, which is in agreement with recent studies that document fractionation during sublimation results in~~ In theory, mechanism 1) causes minimal change in the bulk isotopic composition of a snow layer under isothermal conditions (Ebner et al., 2017). During no SSA decay events did the snow isotopic composition remain consistent. In the case of 2), interstitial diffusion, light isotopes are preferentially diffused, while the heavy isotopes will be preferentially deposited onto the cold snow grains (Colbeck, 1983; Ebner et al., 2017; Touzeau et al., 2016). Thus, diffusion of water vapour in the pore space causes a decrease in d-excess and slight increases in δ^{18}O ~~and decreases in d-excess (Madsen et al., 2019; Hughes et al., 2021; Wahl et al., 2021). However, sublimation is not the only process occurring. Vapour pressure gradients due to surface curvature drive snow metamorphism via vapour diffusion through the pore space and thus, kinetic~~ due to kinetic fractionation (Flanner and Zender, 2006). Similarly, mechanism 3), sublimation, is widely documented to cause an increase in δ^{18}O of the remaining snow-mass due to isotopic fractionation, and a significant decrease in d-excess expected to be due to kinetic fractionation (Ritter et al., 2016; Madsen et al., 2019; Hughes et al., 2021; Wahl et al., 2021; Casado et al., 20 . Conclusively identifying these mechanisms requires water vapour isotopes to model the fractionation ~~is expected to influence the isotopic composition. A larger influence is expected for d-excess than $\delta^{18}O$ because kinetic fractionation influences δD more than $\delta^{18}O$ ($d - excess = \delta D - 8 \cdot \delta^{18}O$) with a stronger influence on d-excess than $\delta^{18}O$, which can explain the covariance between d-excess and SSA observed most clearly during 2019 (Cappa et al., 2003; Dadic et al., 2015). Our approach to the change over a 2-day period instead of daily change allows for increased propagation of the isotope signal~~

during SSA decay to account for the 1 cm representation from Ice Cube SSA measurements, compared to the 2.5 cm bulk isotope measurements (Gallet et al., 2009; Klein, 2014). A significant relationship is observed between change in d-excess and change in SSA effects. In the absence of this data, we infer potential explanations for isotopic change during the low-wind events.

An overall increase in δ^{18}O and decrease in *d*-excess during E10 is likely attributed to a combination of 2) and 3) based on observation of net-sublimation and high amplitude diurnal temperature gradient variability, indicating vapour transport within the pore space. The period between 9th June at 15:18 UTC and 10th June 10:40 UTC had net deposition corresponding to an overall decrease in δ^{18}O during the first 2-days compared to daily analysis (with an additional relationship observed during 2019 between daily change in d-excess and daily change in SSA). Decreases in d-excess are observed during rapid SSA decay, driven by a combination of sublimation, deposition and vapour diffusion through the pore spaceday and minimal decrease in *d*-excess. An increase in snow δ^{18}O would be expected during deposition (Stenni et al., 2016; Feher et al., 2021; Casado et al., 2021) , however, disequilibrium between water vapour isotopic composition and snow isotopic composition may explain the decrease in δ^{18}O (Wahl et al., 2021).

Surface snow metamorphism is not confined to rapid SSA decreases, and thus isotopic composition change is observed continuously . However, results from this study indicate that d-excess changes during Both δ^{18}O and *d*-excess vary continuously throughout June 2018 (Fig. 7), with no clear relationship to total LE or temperature gradients. Strong diurnal surface and subsurface temperature gradients during the low-wind events can explain rapid SSA decay have significantly different distribution than the background non-event fluctuations. Our findings are in agreement with a study from Antarctica which showed a significant relationship between d-excess and physical snow properties with depth, while negligible relationship was observed for δ^{18}O (Dadic et al., 2015). Our study has selected rapid SSA decays fitting to the decay model to address how changes in snow crystal morphology after precipitation relates to change in isotopic composition . Future studies would benefit from using isotope flux models to account for the (Pinzer et al., 2012). We conclude that SSA of the surface snow is strongly influenced by surface-subsurface TG while the changes in isotopic composition are likely to be influenced by other factors such as the magnitude of vapour-snow isotopic disequilibrium during sublimation (Steen-Larsen et al., 2014; Hughes et al., 2021; Wahl et al., 2021) . Decoupling the influence of sublimation and deposition, to determine unexplained isotopic composition change. interstitial diffusion within the snow requires additional measurements of isotopic composition of atmospheric water vapour to model associated fractionation effects (Wahl et al., 2021). Our results suggest that while processes driving SSA decay (snow metamorphism) do modify the isotopic composition of the surface snow, interstitial diffusion has a disproportionate effect on SSA decay.

An additional feature supporting the observation of processes driving surface snow metamorphismcorresponds to a decrease in d-excess, is a clear relationship between substantial increases in SSA and increase in d-excess (Fig. **??**). The upper 10th percentile of ΔSSA increases (14.7

4.2.1 Inter-annual variability

The recurring difference in snow characteristics and temperature conditions during 2019 compared to 2017 and 2018 could be explained by the shifting phase of the North Atlantic Oscillation (NAO) which is in positive phase during 2018 and

2017 (below-average temperatures), and negative phase during 2019. A similar pattern is observed in the snow isotopes when considering the period between 27th May to 1st August where the mean $\delta^{18}O$ values during 2019 was -27.3 ~~$m^2 kg^{-1}$)~~ ~~corresponds to positive Δd-excess in 70‰,~~ which is 4.3 ~~% of cases (Fig. **??**). Large increases in SSA are closely associated with precipitation, however, increases are observed in a number of other scenarios (Domine et al., 2009). Precipitation is expected to cause the largest SSA, suggesting that the d-excess of precipitation is most often higher than existing surface snow. Our results therefore suggest that the precipitation isotopic composition signal is not always preserved after snow metamorphism due to (kinetic) fractionation during sublimation and other surface processes.~~

~~*Change in d-excess per day (Δd-excess day^{-1}) vs. change in SSA per day ($\Delta SSA day^{-1}$)*~~~~The relationship between the rate of change in SSA per day (ΔSSA day^{-1}) and d-excess (Δd-excess day^{-1}) for all summer seasons 2017-2019 (light grey), all events (dark grey) and selected events based on substantial accumulation (dark turquoise). The box indicates the values corresponding to daily decrease in d-excess during decrease in SSA, with 81 % of selected events in this quadrant.~~

4.3 ~~Influence of event conditions on isotopic change~~

~~Surface conditions prior to and during SSA decay eventsvary, with a number of events having no measured accumulation or observed snowfall (Fig. **??**). Removing events with non-homogeneous increases in surface height and events where additional precipitation or significant snowdrift are observed, reveals that during rapid SSA decays following significant precipitation, there is increased likelihood of observing concurrent decrease in d-excess during the first day~~ ‰ higher than 2018 (~~Fig~~-31.6‰) and 3.6‰ higher than 2017 (-30.9‰). While the difference in mean $\delta^{18}O$ can plausibly be explained by a 3.2°C mean air temperature difference, the isotope-SSA covariance is not so straightforward. ~~**??**) . This observation combined with results presented in Fig. **??**a strongly suggests that initial snow metamorphism after precipitation corresponds to a decrease in d-excess of in the surface snow .~~

4.3 ~~Spatial variability of snow surface~~

~~Low accumulation rates at EastGRIP result in the potential for winter snow layers to influence the isotopic composition in the 2.5 cm surface snow. Accumulation heterogeneity causes uneven mixing of layers at each sample site, which is observed clearly in the large spatial variability in isotopic composition measurements in Fig. **??**a and b. EOF analysis is used to account for spatial variability at each site, and a coherence is observed between the principal components of d-excess and SSA.~~

The positive mode of PC1 ~~is weaker when spatial variability is high, and during these periods the coherence between d-excess and SSA are muted. During the start of 2017 and 2018~~ $_{SSA}$ can be interpreted as increases in SSA from depositional events, such as precipitation, surface hoar formation, and wind-fragmented snowdrift (Domine et al., 2009), while the negative mode is associated with snow metamorphism or wind-erosion (Cabanes et al., 2002, 2003; Legagneux et al., 2003, 2004; Taillandier et al., 2007; Fl . Based on this interpretation, a covariance between PC1 ~~of d-excess is coherent with~~ $_{SSA}$ and PC1 ~~of $\delta^{18}O$, and decoupled from PC1 of SSA. At the start of the season, the 2.5 cm sample will contain winter snow layers which are less influenced by snow metamorphism (Libois et al., 2015; Town et al., 2008), and thus, a coherent signal between d-excess and $\delta^{18}O$ is observed. The transition to a coherence between~~ $_{dxs}$ or PC1 ~~of d-excess and PC1 of SSA can be explained by summer snow layers,~~

~~influenced by snow metamorphism, causing d-excess to appear to become decoupled from $\delta^{18}O$, which is less influenced by kinetic fractionation than δD (Masson-Delmotte et al., 2005) during snow metamorphism.~~ $_{\delta^{18}O}$ indicates that the mechanisms controlling SSA variability also influence the isotopic composition.

We observe a decoupling of the temporal variance in *d*-excess from that of δ^{18}O (Fig. 3) in 2019 which is can be attributed to the *d*-excess signal being more sensitive to kinetic effects during sublimation and grain growth between pore air water vapour and the snow grains (Ebner et al., 2017; Casado et al., 2021).

4.3 ~~Implications to ice core interpretation~~

Ongoing work to decouple the processes driving change in isotopic composition - sublimation from surface or interstitial vapour diffusion between layers in the pore space - is vital for precise climate reconstruction in ice cores (Touzeau et al., 2018; Hughes et al., 2021; . Future studies would benefit from obtaining direct measurements of the isotopic composition of precipitation and surface hoar, to determine the fraction of such deposits in the SSA samples. Furthermore, a quantitative representation of vapour fluxes in the surface snow rather than the temperature-gradient based approximation used in this study would provide a basis from which to quantify the relative influence of fractionation during sublimation and interstitial diffusion.

4.3 Implications and perspectives

Documented changes in snow isotopic composition during surface snow metamorphism have potential implications for interpretation of stable water isotope records from ice cores, given that the current interpretation assumes the precipitation signal is preserved (Dansgaard, 1964). ~~Seasonal transition from a coupling of PC1 of d-excess and PC1 of δ^{18}O, to a coherence between PC1 of d-excess PC1 of SSA at the latter part of the season, suggest that summer snow metamorphism causes d-excess to appear to decouple from δ^{18}O. Kinetic fractionation during sublimation is expected to be the cause a decrease in d-excess in the snow, given the different diffusivities of HDO and and $H_2{}^{18}O$ (Masson-Delmotte et al., 2005).~~

~~Seasonal signals are influenced by millennial scale insolation variability (Masson-Delmotte et al., 2006; Laepple et al., 2011) . An inverse relationship is observed between obliquity and d-excess over the past 250ka years at Vostok~~ Variations of *d*-excess in ice core records are attributed to changes in source region, source region conditions and kinetic fractionation occurring during snow crystal formation in supersaturated clouds (Stenni et al., 2010; Jouzel and Merlivat, 1984). However, we show that there are substantial changes in *d*-excess during precipitation-free periods supporting recent work showing that post-depositional factors add complexity to the traditional interpretation of ice core water isotope records. Greenland ice core *d*-excess records show abrupt decreases in *d*-excess corresponding to warming transitions, which is attributed to ~~the insolation gradient between high and low latitudes causing increases moisture transport from low latitudes relative to high latitudes (Vimeux et al., 2001, 1999).~~ change in moisture source regions (Steffensen et al., 2008). Results presented in our study document decreases in snow ~~d-excess~~ *d*-excess during surface snow metamorphism associated with temperature gradients and sublimation, potentially contributing to the total decrease observed in the *d*-excess records. ~~Millennial scale local insolation variability has a strong influence on temperature gradients in the snow (Hutterli et al., 2009). Thus, it is possible that local~~

~~insolation variability may also influence d-excess due to temperature gradients in the snow driving snow metamorphism at the surface.~~

~~Our results highlight the need to consider the influence of surface snow metamorphism on isotopic composition in stable water isotope records as the traditional interpretation of d-excess ice core signal does not account for any post-depositional signal. Future work to decouple the processes driving change in d-excess (sublimation from surface or interstitial vapour diffusion in the pore space) is vital for modelling the change in isotopic composition down to the close-off depth in the firn (Touzeau et al., 2018; Neumann and Waddington, 2004). In addition, it would be beneficial to obtain direct measurements of the isotopic composition and SSA of precipitation , to determine the fraction of precipitation in the SSA samples.~~The findings of this exploratory study reiterate the importance of quantifying the isotopic fractionation effects associated with processes driving snow metamorphism during precipitation-free periods. Moreover, the inter-annual variability observed at EastGRIP between 2018 and 2019 suggests that precipitation intermittency and temperature (gradients) play a role in isotopic change, which is not readily identified in the surface snow SSA data.

5 Conclusions

This study addresses the rapid SSA decay driven by surface snow metamorphism. In particular, the study aims to explore how rapid SSA decay relates to changes in isotopic composition of the surface snow in the dry accumulation zone of the Greenland Ice Sheet. Ten individual snow samples were collected ~~on a daily basis~~ daily over a 90 m transect at EastGRIP in the period between May and August of 2017, 2018 and 2019. SSA and isotopic composition were measured for each sample. Periods of snow metamorphism after ~~precipitation events are~~ deposition events were defined using SSA measurements to extract periods of rapid decreases in SSA.

An exponential SSA decay model (~~$SSA(t) = (SSA_0 - 26.8)e^{-0.54t} + 26.8$~~$SSA(t) = (SSA_0 - 22) \cdot e^{-\alpha \cdot t} + 22$) was constructed to describe surface snow metamorphism ~~under mean~~ in summer conditions for polar snow, with surface temperatures ~~between -25~~above -20 °C and ~~0~~with minimal surface perturbation. Two event categories were defined based on wind speed, with an upper threshold of 7 ~~°C and wind speeds below 6 $m\,s^{-1}$. The empirical model can be applied to remote areas of polar ice sheets and requires only initial SSA as the parameter, making it simple to use. The relationship between defined events of snow metamorphism and corresponding snow isotopic composition was then explored~~$\mathrm{m\,s^{-1}}$ to minimise chance of snowdrift. Wind speed is observed to increase surface SSA decay rate showing that snow metamorphism is enhanced with increased ventilation.

~~We observe changes~~ Changes in isotopic composition corresponding to post-depositional processes driving ~~rapid SSA decay~~ SSA decay are observed in all low- and moderate-wind events. A decrease in d-excess from day-0 to day-2 is observed in 4 out of the 6 events with no precipitation. ~~Principal components from EOF analysis for SSA and d-excess indicate that under near-homogeneous surface snow conditions, d-excess varies in phase with SSA throughout a large proportion of the sampling seasons. This suggests that post-depositional processes and precipitationinfluence both physical snow structure and isotopic composition concurrently. Over the first 2-days of rapid~~ Further analysis of low-wind SSA decay events ~~, d-excess is observed~~

~~to decrease significantly from the initial value for most events, at the same time we observe net sublimation. Significant changes in surface snow d-excess are observed during days following a precipitation event, suggesting that precipitation d-excess signal is altered after deposition, together with changes in physical snow properties (SSA).~~ indicates that the combined effects of vapour diffusion and diurnal LE variability causes isotopic fractionation of the surface snow in the absence of precipitation. The differing fractionation effects are expected to be the result of vapour-snow isotopic disequilibrium. A strong correlation observed between SSA and *d*-excess found in 2019 was not present for 2018. We suggest that this is due to strong sublimation corresponding to high temperatures during 2019.

In summary, our results ~~suggest~~ support documentation of fractionation during sublimation and deposition between the snow surface and atmosphere, indicating that the precipitation isotopic composition signal is not always preserved ~~due to isotopic fractionation~~ during the processes driving surface snow metamorphism. Observations of post-depositional decrease in ~~d-excess~~ *d*-excess during rapid SSA decay hints to local processes influencing the ~~d-excess~~ *d*-excess signal and therefore an interpretation as source region signal ~~is implausible~~alone is insufficient.

Appendix A

Table A1. ~~*SSA Decay Event Conditions*~~Description of conditions for SSA decays captured by decrease threshold. Duration and conditions for all 21 events defined by the threshold. ~~'Initial Conditions' refers to~~ Observations were made of snowfall, snowdrift and ground fog. Presented here are the conditions during the day (-24h) ~~before the~~ preceding each event (Initial conditions), ~~while 'Event Conditions' describes~~ the dominant conditions ~~for~~ throughout the event ~~duration,~~ (Sky conditions) and observations of surface perturbations (Comments). based on field observations.~~'Surface Temperature' is the mean surface temperature during the event. 'Comments' highlight any significant weather behaviour during the event.~~

	Date	Event No.	Surface ~~Temperature~~ temp. (°C)	Initial ~~Conditions~~ conditions	~~Event Conditions~~ Sky conditions
2017	27/05 - ~~01~~31/~~06~~ 05	E1	-17.3	No clear driver	Clear-sky
	19/06 - 24/06	E2	-13.6	Snowfall	Clear-sky
	30/06 - 02/07	E3	-14.0	Snowfall	Overcast
	10/07 - 15/07	E4	-13.2	Snowfall	Clear-sky
	18/07 - 19/07	E5	-11.7	Snowfall	Overcast
	21/07 - 23/07	E6	-11.2	Snowfall	Overcast
2018	07/05 - 10/05	E7	-33.7	Drift and fog	Clear/ice-fog
	14/05 - 15/05	E8	-19.8	Snowfall	Clear-sky
	16/05 - 18/05	E9	-21.5	Snowfall and fog	Overcast
	09/06 - 11/06	E10	-14.9	~~Ground fog~~ Snowfall	Overcast
	27/06 - 29/06	E11	-15.3	Ground fog	Clear-sky
	30/06 - 03/07	E12	-11.2	Wind drifted snow	Clear-sky
	04/07 - 06/07	E13	-10.2	Snowfall	Clear-sky
	16/07 - 21/07	E14	-14.3	No clear driver	Clear-sky
	23/07 - 27/07	E15	-14.1	Ground fog	Clear-sky
2019	17/06 - 20/06	E16	-11.4	Snowfall	Clear-sky
	27/06 - 30/06	E17	-9.5	No clear driver	Overcast
	02/07 - 05/07	E18	-7.0	Snowfall	Overcast
	06/07 - 08/07	E19	-10.0	No clear driver	Clear-sky
	18/07 - 20/07	E20	-7.6	Ground fog	Overcast
	28/07 - 31/07	E21	-6.5	No clear driver	Clear-sky

~~*Accumulation at each sample site*~~Accumulation measurements from each sample site over the 90 m sampling transect is shown here for 2017, 2018 and 2019 respectively. Each line represents an individual site. Negative values indicate a decrease in surface height, and positive values suggest precipitation or deposition adding to the surface height. The grey bars show the individual events defined in Section 3.1

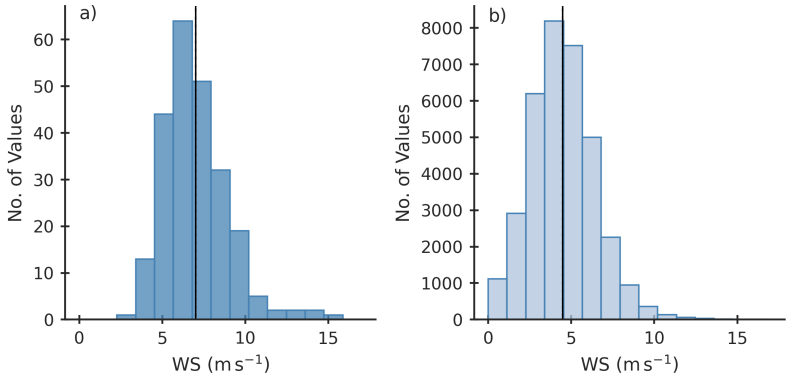

Figure A1. *Wind-speed Distribution*
Histograms showing a) the daily maximum values and b) the 10-minute mean values for all sampling days of 2017, 2018 and 2019. The black line indicates the mean.

Data availability. The SSA, density and accumulation data for all sampling years is available on the PANGAEA database with the DOI:***. Snow isotope data is also available on the PANGAEA database with the DOI:***. Data from the Programme for Monitoring of the Greenland Ice Sheet (PROMICE) 400 were provided by the Geological Survey of Denmark and Greenland (GEUS) at http://www.promice.dk. Eddy Covaraniance Tower measurement are available on the PANGAEA database with the DOI: https://doi.org/10.1594/PANGAEA.928827.

Author contributions. HCSL, AKF and RHS designed the study together. AKF, SW, MH, MB, AZ, SK and HCSL carried out the data collection and measurements. RHS, AKF and HCSL worked directly with the data. RHS, AKF and HCSL prepared the manuscript with contributions from all co-authors. AKF contributed largely to the manuscript text and structure. HCSL designed and administrated the SNOWISO project.

Competing interests. The authors declare that they have no conflict of interest.

Acknowledgements. This project has received funding from the European Research Council (ERC) under the European Union's Horizon 2020 research and innovation program: Starting Grant-SNOWISO (grant agreement 759526). EastGRIP is directed and organized by the Centre for Ice and Climate at the Niels Bohr Institute, University of Copenhagen. It is supported by funding agencies and institutions in Denmark (A. P. Møller Foundation, University of Copen-hagen), USA (US National Science Foundation, Office of Polar Programs), Germany (Alfred Wegener Institute, Helmholtz Centre for Polar and Marine Research), Japan (National Institute of Polar Research and Arctic Challenge for Sustainability), Norway (University of Bergen and Bergen Research Foun-dation), Switzerland (Swiss National Science

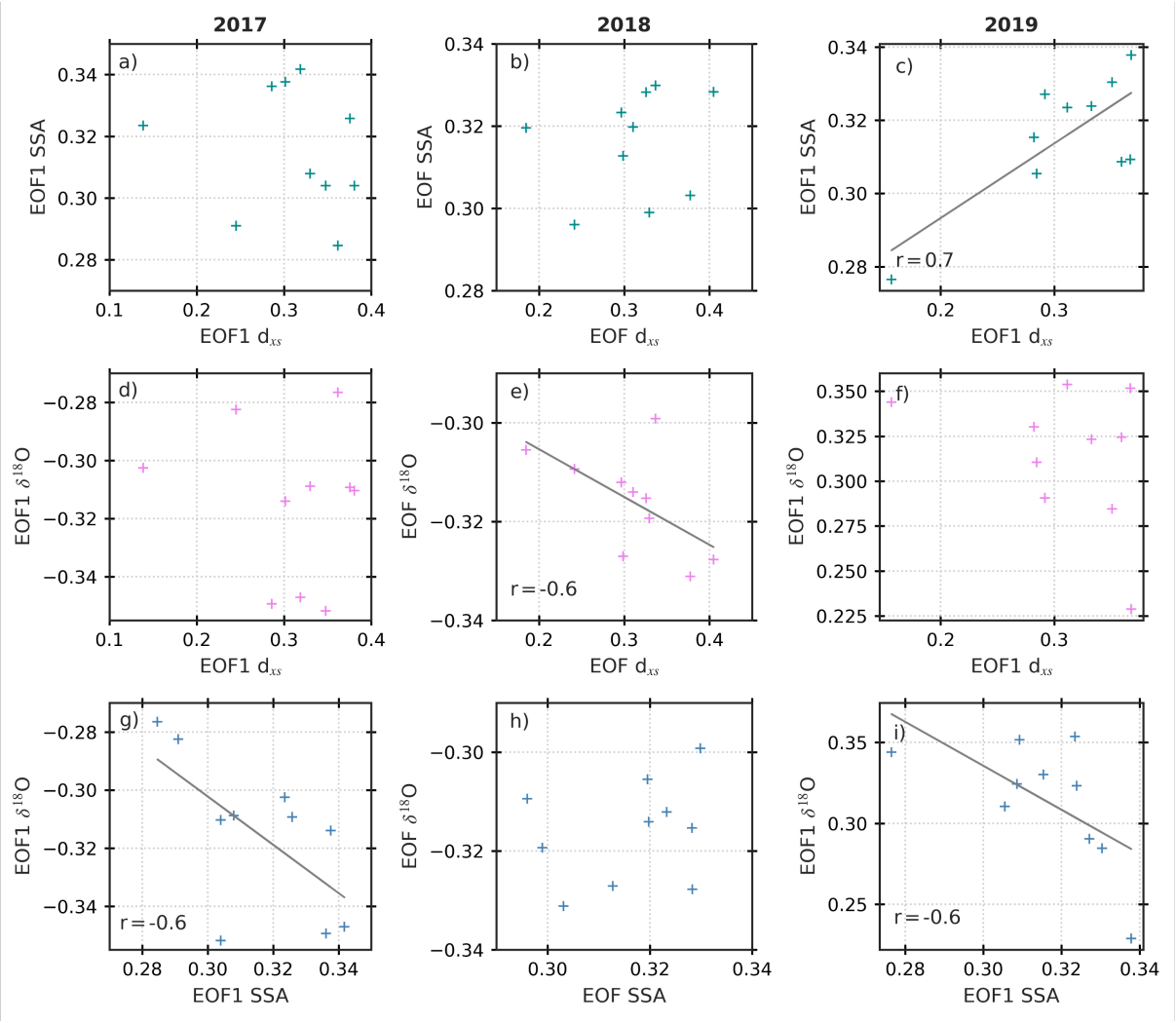

Figure A2. Results from the EOF analysis showing the relationship between SSA, *d*-excess and $\delta^{18}O$ in the spatial dimension. Linear regressions are included in plots with significant correlations ($p<0.05$) between variables.

Foundation), France (French Polar Institute Paul-Emile Victor, Insti-tute for Geosciences and Environmental research), and China (Chinese Acad-emy of Sciences and Beijing Normal University).

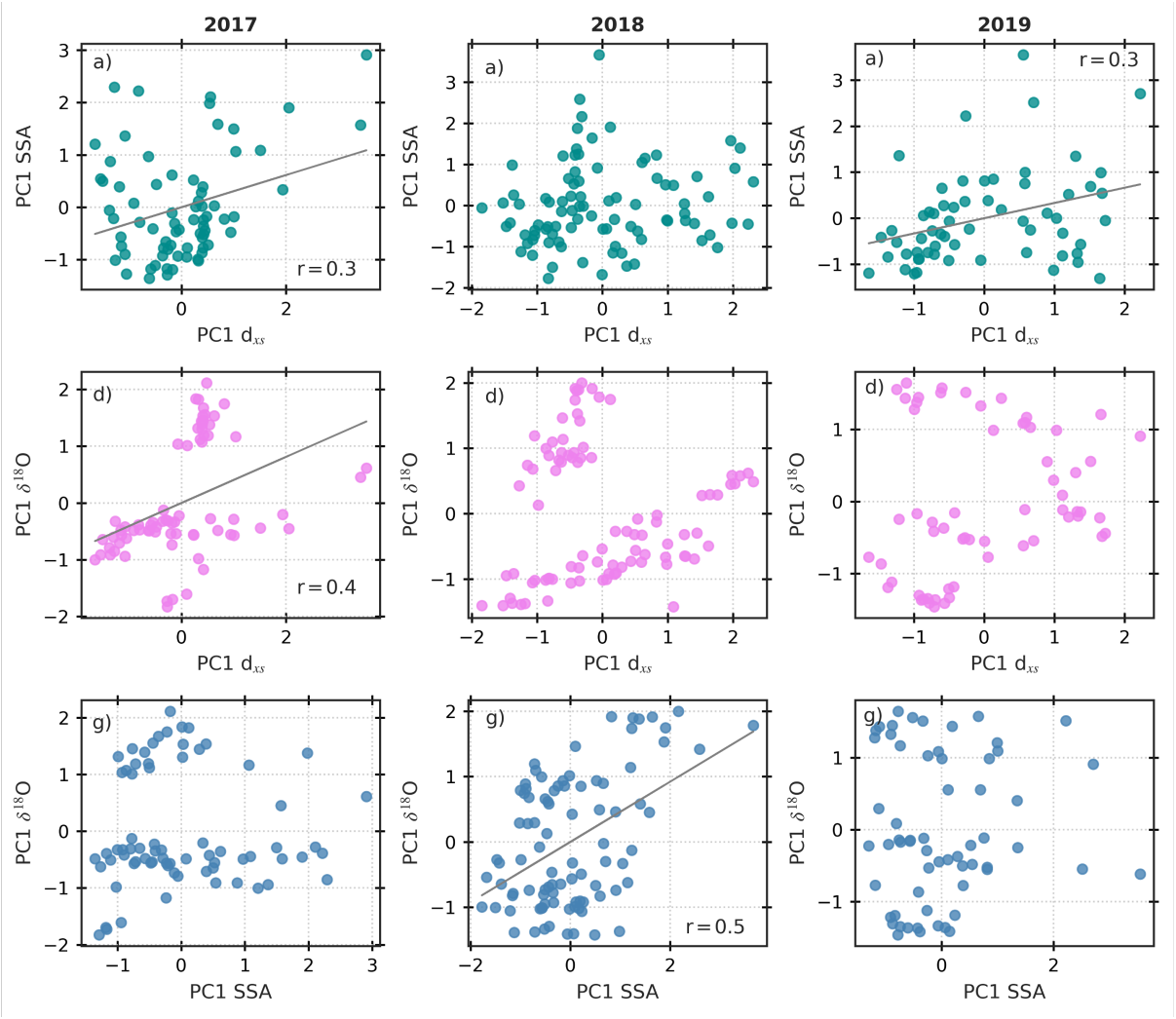

Figure A3. Results from the EOF analysis showing the relationship between SSA, *d*-excess and δ^{18}O in the temporal dimension. Linear regressions are included in plots with significant correlations ($p<0.05$) between variables.

References

Birnbaum, G., Freitag, J., Brauner, R., Ko¨nig, G., Ko¨nig-Langlo, K., Schulz, E., Kipfstuhl, S., Oerter, H., Reijmer, C. H., Schlosser, E., Faria, S. H., Ries, H., Loose, B., Herber, A., Duda, M. G., Powers, J. G., Manning, K. W., and Van Den Broeke, M. R.: Strong-wind events and their influence on the formation of snow dunes: observations from Kohnen station, Dronning Maud Land, Antarctica, Journal of Glaciology, 56, 891–902, https://www.cambridge.org/core., 2010.

Cabanes, A., Legagneux, L., and Dominé, F.: Evolution of the specific surface area and of crystal morphology of Arctic fresh snow during the ALERT 2000 campaign, Atmospheric Environment, 36, 2767–2777, https://doi.org/10.1016/S1352-2310(02)00111-5, 2002.

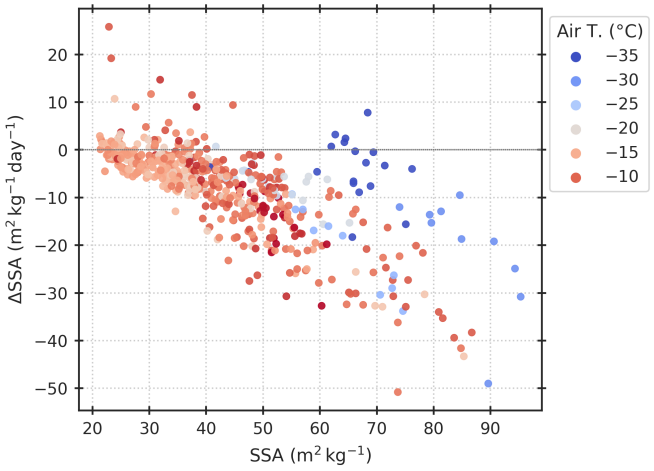

Figure A4. The derivative of SSA is shown as a function of SSA. All events captured by the decrease threshold are included here. The markers are coloured by mean air temperature between sampling.

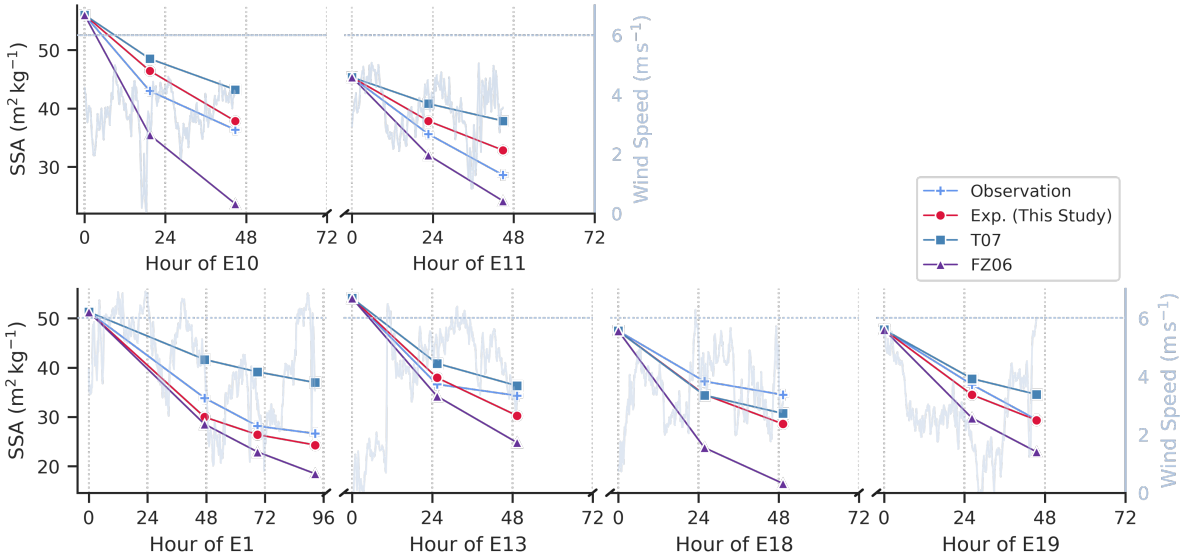

Figure A5. SSA decay model evaluation and a comparison to observations. Included models are the decay model from this study and the existing decay models from Flanner and Zender (2006), FZ06, and Taillandier et al. (2007), T07. The 10-minute averaged wind-speed is shown on the secondary y-axis, with the 6 $m^2 kg^{-1}$ thresholds indicated. Low-wind events E10 and E11 are shown in the upper panel, and moderate-wind events are shown in the lower panel (E1, E13, E18 and E19).

Cabanes, A., Legagneux, L., and Dominé, F.: Rate of evolution of the specific surface area of surface snow layers, Environmental Science and Technology, 37, 661–666, https://doi.org/10.1021/es025880r, 2003.

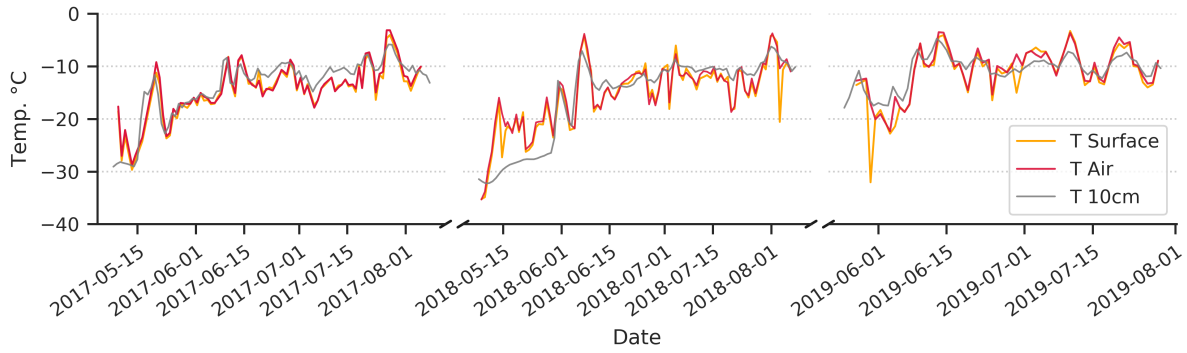

Figure A6. Daily mean air, surface and subsurface temperature time-series for 2017, 2018 and 2019.

Cappa, C. D., Hendricks, M. B., DePaolo, D. J., and Cohen, R. C.: Isotopic fractionation of water during evaporation, Journal of Geophysical Research: Atmospheres, 108, https://doi.org/10.1029/2003jd003597, 2003.

Carmagnola, C. M., Domine, F., Dumont, M., Wright, P., Strellis, B., Bergin, M., Dibb, J., Picard, G., Libois, Q., Arnaud, L., and Morin, S.: Snow spectral albedo at Summit, Greenland: Measurements and numerical simulations based on physical and chemical properties of the snowpack, Cryosphere, 7, 1139–1160, https://doi.org/10.5194/tc-7-1139-2013, 2013.

Casado, M., Landais, A., Picard, G., Münch, T., Laepple, T., Stenni, B., Dreossi, G., Ekaykin, A., Arnaud, L., Genthon, C., Touzeau, A., Masson-Delmotte, V., and Jouzel, J.: Archival processes of the water stable isotope signal in East Antarctic ice cores, Cryosphere, 12, 1745–1766, https://doi.org/10.5194/tc-12-1745-2018, 2018.

Casado, M., Münch, T., and Laepple, T.: Climatic information archived in ice cores: Impact of intermittency and diffusion on the recorded isotopic signal in Antarctica, Climate of the Past, 16, 1581–1598, https://doi.org/10.5194/cp-16-1581-2020, 2020.

Casado, M., Landais, A., Picard, G., Arnaud, L., Dreossi, G., Stenni, B., and Prié, F.: Water Isotopic Signature of Surface Snow Metamorphism in Antarctica, Geophysical Research Letters, 48, https://doi.org/10.1029/2021GL093382, 2021.

Christiansen, H. H.: Snow-cover depth, distribution and duration data from northeast Greenland obtained by continuous automatic digital photography, Annals of Glaciology, 32, 102–108, https://www.cambridge.org/core., 2001.

Ciais, P. and Jouzel, J.: Deuterium and oxygen 18 in precipitation: Isotopic model, including mixed cloud processes, Tech. Rep. D8, 1994.

Colbeck, S. C.: Thermodynamics of snow metamorphism due to variations in curvature, Journal of Glaciology, 26, 291–301, https://www.cambridge.org/core., 1980.

Colbeck, S. C.: Theory of metamorphism of dry snow., Journal of Geophysical Research, 88, 5475–5482, https://doi.org/10.1029/JC088iC09p05475, 1983.

Comola, F., Kok, J. F., Gaume, J., Paterna, E., and Lehning, M.: Fragmentation of wind-blown snow crystals, Geophysical Research Letters, 44, 4195–4203, https://doi.org/10.1002/2017GL073039, 2017.

Dadic, R., Schneebeli, M., Bertler, N. A., Schwikowski, M., and Matzl, M.: Extreme snow metamorphism in the Allan Hills, Antarctica, as an analogue for glacial conditions with implications for stable isotope composition, Journal of Glaciology, 61, 1171–1182, https://doi.org/10.3189/2015JoG15J027, 2015.

Dansgaard, W.: Stable isotopes in precipitation, Tellus, 16, 436–468, https://doi.org/10.3402/tellusa.v16i4.8993, 1964.

Domine, F., Taillandier, A. S., and Simpson, W. R.: A parameterization of the specific surface area of seasonal snow for field use and for models of snowpack evolution, Journal of Geophysical Research: Earth Surface, 112, 1–13, https://doi.org/10.1029/2006JF000512, 2007.

Domine, F., Albert, M., Huthwelker, T., Jacobi, H.-W., Kokhanovsky, A. A., Lehning, M., Picard, G., and Simpson, W. R.: Snow physics as relevant to snow photochemistry, Tech. rep., www.atmos-chem-phys.net/8/171/2008/, 2008.

Domine, F., Taillandier, A. S., Cabanes, A., Douglas, T. A., and Sturm, M.: Three examples where the specific surface area of snow increased over time, Cryosphere, 3, 31–39, https://doi.org/10.5194/tc-3-31-2009, 2009.

Ebner, P. P., Steen-Larsen, H. C., Stenni, B., Schneebeli, M., and Steinfeld, A.: Experimental observation of transient δ18O interaction between snow and advective airflow under various temperature gradient conditions, The Cryosphere Discussions, pp. 1–36, https://doi.org/10.5194/tc-2017-16, 2017.

Faber, A. K., Vinther, B. M., Sjolte, J., and Pedersen, R. A.: How does sea ice influence δ18O of Arctic precipitation?, Atmospheric Chemistry and Physics, 17, 5865–5876, https://doi.org/10.5194/acp-17-5865-2017, 2017.

Fausto, R. S., Van As, D., Mankoff, K. D., Vandecrux, B., Citterio, M., Ahlstrøm, A. P., Andersen, S. B., Colgan, W., Karlsson, N. B., Kjeldsen, K. K., Korsgaard, N. J., Larsen, S. H., Nielsen, S., Pedersen, A. , Shields, C. L., Solgaard, A. M., and Box, J. E.: PROMICE automatic weather station data, Earth System Science Data, 80, 1–41, https://doi.org/10.22008/promice/data/aws, 2021.

Feher, R., Voiculescu, M., Chiroiu, P., and Perșoiu, A.: The stable isotope composition of hoarfrost, https://doi.org/10.1080/10256016.2021.1917567, 2021.

Flanner, M. G. and Zender, C. S.: Linking snowpack microphysics and albedo evolution, Journal of Geophysical Research Atmospheres, 111, 1–12, https://doi.org/10.1029/2005JD006834, 2006.

Flin, F. and Brzoska, J. B.: The temperature-gradient metamorphism of snow: Vapour diffusion model and application to tomographic images, Annals of Glaciology, 49, 17–21, https://doi.org/10.3189/172756408787814834, 2008.

Gallet, J. C., Domine, F., Zender, C. S., and Picard, G.: Measurement of the specific surface area of snow using infrared reflectance in an integrating sphere at 1310 and 1550 nm, Cryosphere, 3, 167–182, https://doi.org/10.5194/tc-3-167-2009, 2009.

Gallet, J. C., Domine, F., Arnaud, L., Picard, G., and Savarino, J.: Vertical profile of the specific surface area and density of the snow at Dome C and on a transect to Dumont D'Urville, Antarctica - Albedo calculations and comparison to remote sensing products, Cryosphere, 5, 631–649, https://doi.org/10.5194/tc-5-631-2011, 2011.

Gallet, J. C., Domine, F., Savarino, J., Dumont, M., and Brun, E.: The growth of sublimation crystals and surface hoar on the Antarctic plateau, Cryosphere, 8, 1205–1215, https://doi.org/10.5194/tc-8-1205-2014, 2014.

Genthon, C., Piard, L., Vignon, E., Madeleine, J. B., Casado, M., and Gallée, H.: Atmospheric moisture supersaturation in the near-surface atmosphere at Dome C, Antarctic Plateau, Atmospheric Chemistry and Physics, 17, 691–704, https://doi.org/10.5194/acp-17-691-2017, 2017.

Holme, C., Gkinis, V., and Vinther, B. M.: Molecular diffusion of stable water isotopes in polar firn as a proxy for past temperatures, Geochimica et Cosmochimica Acta, 225, 128–145, https://doi.org/10.1016/j.gca.2018.01.015, 2018.

Hughes, A. G., Wahl, S., Jones, T. R., Zuhr, A., Hörhold, M., White, J. W. C., and Steen-Larsen, H. C.: The role of sublimation as a driver of climate signals in the water isotope content of surface snow: Laboratory and field experimental results, The Cryosphere, https://doi.org/10.5194/tc-2021-87, 2021.

Hutterli, M. A., Schneebcli, M., Freitag, J., Kipfstuhl, J., and Rothlisberger, R.: Impact of Local Insolation on Snow Metamorphism and Ice Core Records, Hokkaido University, 68, 223–232, https://doi.org/http://hdl.handle.net/2115/45450, 2009.

Johnsen, S. ., Clausen, H. B., Cuffey, K. M., Hoffmann, G., Schwander, J., and Creyts, T.: Diffusion of stable isotopes in polar firn and ice: the isotope effect in firn diffusion, Physics of Ice Core Records, pp. 121–142, 2000.

Johnsen, S. J., Dansgaard, W., and White, J. W.: The origin of Arctic precipitation under present and glacial conditions, Tellus, Series B, 41 B, 452–468, https://doi.org/10.3402/tellusb.v41i4.15100, 1989.

Jouzel, J. and Merlivat, L.: Deuterium and oxygen 18 in precipitation: modeling of the isotopic effects during snow formation., Journal of Geophysical Research, 89, 749–757, https://doi.org/10.1029/jd089id07p11749, 1984.

Klein, K.: Variability in dry Antarctic firn - Investigations on spatially distributed snow and firn samples from Dronning Maud Land, Antarctica, PhD Thesis, University of Bremen, 3, 1–15, https://doi.org/10.1016/j.cell.2009.01.043, 2014.

Kokhanovsky, A., Lamare, M., Danne, O., Brockmann, C., Dumont, M., Picard, G., Arnaud, L., Favier, V., Jourdain, B., Meur, E. L., Di Mauro, B., Aoki, T., Niwano, M., Rozanov, V., Korkin, S., Kipfstuhl, S., Freitag, J., Hoerhold, M., Zuhr, A., Vladimirova, D., Faber, A. K., Steen-Larsen, H. C., Wahl, S., Andersen, J. K., Vandecrux, B., van As, D., Mankoff, K. D., Kern, M., Zege, E., and Box, J. E.: Retrieval of snow properties from the Sentinel-3 Ocean and Land Colour Instrument, Remote Sensing, 11, https://doi.org/10.3390/rs11192280, 2019.

Laepple, T., Werner, M., and Lohmann, G.: Synchronicity of Antarctic temperatures and local solar insolation on orbital timescales, Nature, 471, 91–94, https://doi.org/10.1038/nature09825, 2011.

Laepple, T., Münch, T., Casado, M., Hoerhold, M., Landais, A., and Kipfstuhl, S.: On the similarity and apparent cycles of isotopic variations in East Antarctic snow pits, Cryosphere, 12, 169–187, https://doi.org/10.5194/tc-12-169-2018, 2018.

Landais, A., Barnola, J. M., Kawamura, K., Caillon, N., Delmotte, M., Van Ommen, T., Dreyfus, G., Jouzel, J., Masson-Delmotte, V., Minster, B., Freitag, J., Leuenberger, M., Schwander, J., Huber, C., Etheridge, D., and Morgan, V.: Firn-air δ15N in modern polar sites and glacial-interglacial ice: A model-data mismatch during glacial periods in Antarctica?, Quaternary Science Reviews, 25, 49–62, https://doi.org/10.1016/j.quascirev.2005.06.007, 2006.

Legagneux, L. and Domine, F.: A mean field model of the decrease of the specific surface area of dry snow during isothermal metamorphism, Journal of Geophysical Research: Earth Surface, 110, https://doi.org/10.1029/2004JF000181, 2005.

Legagneux, L., Cabanes, A., and Dominé, F.: Measurement of the specific surface area of 176 snow samples using methane adsorption at 77 K, Journal of Geophysical Research Atmospheres, 107, 5–1, https://doi.org/10.1029/2001JD001016, 2002.

Legagneux, L., Lauzier, T., Dominé, F., Kuhs, W. F., Heinrichs, T., and Techmer, K.: Rate of decay of specific surface area of snow during isothermal experiments and morphological changes studied by scanning electron microscopy, Canadian Journal of Physics, 81, 459–468, https://doi.org/10.1139/p03-025, 2003.

Legagneux, L., Taillandier, A. S., and Domine, F.: Grain growth theories and the isothermal evolution of the specific surface area of snow, Journal of Applied Physics, 95, 6175–6184, https://doi.org/10.1063/1.1710718, 2004.

Li, L. and Pomeroy, J. W.: Estimates of threshold wind speeds for snow transport using meteorological data, Journal of Applied Meteorology, 36, 205–213, https://doi.org/10.1175/1520-0450(1997)036<0205:EOTWSF>2.0.CO;2, 1997.

Libois, Q., Picard, G., Arnaud, L., Morin, S., and Brun, E.: Modeling the impact of snow drift on the decameter-scale variability of snow properties on the Antarctic Plateau, Journal of Geophysical Research, 119, 662–11, https://doi.org/10.1002/2014JD022361, 2014.

Libois, Q., Picard, G., Arnaud, L., Dumont, M., Lafaysse, M., Morin, S., and Lefebvre, E.: Summertime evolution of snow specific surface area close to the surface on the Antarctic Plateau, Cryosphere, 9, 2383–2398, https://doi.org/10.5194/tc-9-2383-2015, 2015.

Linow, S., Hörhold, M. W., and Freitag, J.: Grain-size evolution of polar firn: A new empirical grain growth parameterization based on X-ray microcomputer tomography measurements, Journal of Glaciology, 58, 1245–1252, https://doi.org/10.3189/2012JoG11J256, 2012.

Madsen, M. V., Steen-Larsen, H. C., Hörhold, M., Box, J., Berben, S. M., Capron, E., Faber, A. K., Hubbard, A., Jensen, M. F., Jones, T. R., Kipfstuhl, S., Koldtoft, I., Pillar, H. R., Vaughn, B. H., Vladimirova, D., and Dahl-Jensen, D.: Evidence of Isotopic Fractionation During Vapor Exchange Between the Atmosphere and the Snow Surface in Greenland, Journal of Geophysical Research: Atmospheres, 124, 2932–2945, https://doi.org/10.1029/2018JD029619, 2019.

Masson-Delmotte, V., Landais, A., Stievenard, M., Cattani, O., Falourd, S., Jouzel, J., Johnsen, S. J., Dahl-Jensen, D., Sveinsbjornsdottir, A., White, J. W., Popp, T., and Fischer, H.: Holocene climatic changes in Greenland: Different deuterium excess signals at Greenland Ice Core Project (GRIP) and NorthGRIP, Journal of Geophysical Research D: Atmospheres, 110, 1–13, https://doi.org/10.1029/2004JD005575, 2005.

Masson-Delmotte, V., Dreyfus, G., Braconnot, P., Johnsen, S., Jouzel, J., Kageyama, M., Landais, A., Loutre, M.-F., Nouet, J., Parrenin, F., Raynaud, D., Stenni, B., and Tuenter, E.: Climate of the Past Past temperature reconstructions from deep ice cores: relevance for future climate change, Tech. rep., www.clim-past.net/2/145/2006/, 2006.

Merlivat, L. and Jouzel, J.: Global climatic interpretation of the deuterium-oxygen 16 relationship for precipitation., Journal of Geophysical Research, 84, 5029–5033, https://doi.org/10.1029/JC084iC08p05029, 1979.

Neumann, T. A. and Waddington, E. D.: Effects of firn ventilation on isotopic exchange, Journal of Glaciology, 50, 183–194, https://www.cambridge.org/core., 2004.

Neumann, T. A., Albert, M. R., Engel, C., Courville, Z., and Perron, F.: Sublimation rate and the mass-transfer coefficient for snow sublimation, International Journal of Heat and Mass Transfer, 52, 309–315, https://doi.org/10.1016/j.ijheatmasstransfer.2008.06.003, 2009.

Picard, G., Royer, A., Arnaud, L., and Fily, M.: Influence of meter-scale wind-formed features on the variability of the microwave brightness temperature around Dome C in Antarctica, Cryosphere, 8, 1105–1119, https://doi.org/10.5194/tc-8-1105-2014, 2014.

Picard, G., Arnaud, L., Caneill, R., Lefebvre, E., and Lamare, M.: Observation of the process of snow accumulation on the Antarctic Plateau by time lapse laser scanning, Cryosphere, 13, 1983–1999, https://doi.org/10.5194/tc-13-1983-2019, 2019.

Pinzer, B. and Schneebeli, M.: Temperature gradient metamorphism is not a classical coarsening process, ISSW 09 - International Snow Science Workshop, Proceedings, pp. 58–61, 2009a.

Pinzer, B. R. and Schneebeli, M.: Snow metamorphism under alternating temperature gradients: Morphology and recrystallization in surface snow, Geophysical Research Letters, 36, 10–13, https://doi.org/10.1029/2009GL039618, 2009b.

Pinzer, B. R., Schneebeli, M., and Kaempfer, T. U.: Vapor flux and recrystallization during dry snow metamorphism under a steady temperature gradient as observed by time-lapse micro-tomography, Cryosphere, 6, 1141–1155, https://doi.org/10.5194/tc-6-1141-2012, 2012.

Ritter, F., Christian Steen-Larsen, H., Werner, M., Masson-Delmotte, V., Orsi, A., Behrens, M., Birnbaum, G., Freitag, J., Risi, C., and Kipfstuhl, S.: Isotopic exchange on the diurnal scale between near-surface snow and lower atmospheric water vapor at Kohnen station, East Antarctica, Cryosphere, 10, 1647–1663, https://doi.org/10.5194/tc-10-1647-2016, 2016.

Schaller, C. F., Freitag, J., and Eisen, O.: Critical porosity of gas enclosure in polar firn independent of climate, Climate of the Past, 13, 1685–1693, https://doi.org/10.5194/cp-13-1685-2017, 2017.

Sime, L. C., Risi, C., Tindall, J. C., Sjolte, J., Wolff, E. W., Masson-delmotte, V., and Capron, E.: Warm climate isotopic simulations : what do we learn about interglacial signals in Greenland ice cores ?, Quaternary Science Reviews, 67, 59–80, https://doi.org/10.1016/j.quascirev.2013.01.009, 2013.

Sodemann, H., Masson-Delmotte, V., Schwierz, C., Vinther, B. M., and Wernli, H.: Interannual variability of Greenland winter precipitation sources: 2. Effects of North Atlantic Oscillation variability on stable isotopes in precipitation, Journal of Geophysical Research Atmospheres, 113, 1–21, https://doi.org/10.1029/2007JD009416, 2008.

Sokratov, S. A. and Golubev, V. N.: Snow isotopic content change by sublimation, Journal of Glaciology, 55, 823–828, https://doi.org/10.3189/002214309790152456, 2009.

Steen-Larsen, H. C., Sveinbjörnsdottir, A. E., Peters, A. J., Masson-Delmotte, V., Guishard, M. P., Hsiao, G., Jouzel, J., Noone, D., Warren, J. K., and White, J. W.: Climatic controls on water vapor deuterium excess in the marine boundary layer of the North Atlantic based on 500 days of in situ, continuous measurements, Atmospheric Chemistry and Physics, 14, 7741–7756, https://doi.org/10.5194/acp-14-7741-2014, 2014.

Steffensen, J. P., Andersen, K. K., Bigler, M., Clausen, H. B., Dahl-Jensen, D., Fischer, H., Goto-Azuma, K., Hansson, M., Johnsen, S. J., Jouzel, J., Masson-Delmotte, V., Popp, T., Rasmussen, S. O., Röthlisberger, R., Ruth, U., Stauffer, B., Siggaard-Andersen, M. L., Sveinbjörnsdottir, E., Svensson, A., and White, J. W.: High-resolution greenland ice core data show abrupt climate change happens in few years, Science, 321, 680–684, https://doi.org/10.1126/science.1157707, 2008.

Stenni, B., Masson-Delmotte, V., Selmo, E., Oerter, H., Meyer, H., Röthlisberger, R., Jouzel, J., Cattani, O., Falourd, S., Fischer, H., Hoffmann, G., Iacumin, P., Johnsen, S. J., Minster, B., and Udisti, R.: The deuterium excess records of EPICA Dome C and Dronning Maud Land ice cores (East Antarctica), Quaternary Science Reviews, 29, 146–159, https://doi.org/10.1016/j.quascirev.2009.10.009, 2010.

Stenni, B., Scarchilli, C., Masson-Delmotte, V., Schlosser, E., Ciardini, V., Dreossi, G., Grigioni, P., Bonazza, M., Cagnati, A., Karlicek, D., Risi, C., Udisti, R., and Valt, M.: Three-year monitoring of stable isotopes of precipitation at Concordia Station, East Antarctica, Cryosphere, 10, 2415–2428, https://doi.org/10.5194/tc-10-2415-2016, 2016.

Taillandier, A. S., Domine, F., Simpson, W. R., Sturm, M., and Douglas, T. A.: Rate of decrease of the specific surface area of dry snow: Isothermal and temperature gradient conditions, Journal of Geophysical Research: Earth Surface, 112, 1–13, https://doi.org/10.1029/2006JF000514, 2007.

Touzeau, A., Landais, A., Stenni, B., Uemura, R., Fukui, K., Fujita, S., Guilbaud, S., Ekaykin, A., Casado, M., Barkan, E., Luz, B., Magand, O., Teste, G., Le Meur, E., Baroni, M., Savarino, J., Bourgeois, I., and Risi, C.: Acquisition of isotopic composition for surface snow in East Antarctica and the links to climatic parameters, Cryosphere, 10, 837–852, https://doi.org/10.5194/tc-10-837-2016, 2016.

Touzeau, A., Landais, A., Morin, S., Arnaud, L., and Picard, G.: Numerical experiments on vapor diffusion in polar snow and firn and its impact on isotopes using the multi-layer energy balance model Crocus in SURFEX v8.0, Geoscientific Model Development, 11, 2393–2418, https://doi.org/10.5194/gmd-11-2393-2018, 2018.

Town, M. S., Waddington, E. D., Walden, V. P., and Warren, S. G.: Temperatures, heating rates and vapour pressures in near-surface snow at the South Pole, Tech. Rep. 186, 2008.

Van As, D.: Warming, glacier melt and surface energy budget from weather station observations in the Melville Bay region of northwest Greenland, Journal of Glaciology, 47, https://www.cambridge.org/core., 2011.

Van Geldern, R. and Barth, J. A.: Optimization of instrument setup and post-run corrections for oxygen and hydrogen stable isotope measurements of water by isotope ratio infrared spectroscopy (IRIS), Limnology and Oceanography: Methods, 10, 1024–1036, https://doi.org/10.4319/lom.2012.10.1024, 2012.

Vimeux, F., Masson, V., Jouzel, J., Stievenard, M., and Petit, J. R.: Glacial-interglacial changes in ocean surface conditions in the Southern Hemisphere, Nature, 398, 410–413, 1999.

Vimeux, F., Masson, V., Delaygue, G., Jouzel, J., Petit, J. R., and Stievenard, M.: A 420,000 year deuterium excess record from East Antarctica: Information on past changes in the origin of precipitation at Vostok, Journal of Geophysical Research Atmospheres, 106, 31 863–31 873, https://doi.org/10.1029/2001JD900076, 2001.

Vinther, B. M., Buchardt, S., Clausen, H., Dahl-Jensen, D., Johnsen, S., Fisher, D., Koerner, R., Raynaud, D., Lipenkov, V., Andersen, K., Blunier, T., Rasmussen, S., Steffensen, J., and Svensson, A.: Holocene thinning of the Greenland ice sheet, Nature, 461, 385–388, 2009.

Wahl, S., Steen-Larsen, H. C., and Reuder, J.: Quantifying the Stable Water Isotopologue Exchange between Snow Surface and Lower Atmosphere by Direct Flux Measurements, Journal of Geophysical Research: Atmospheres, https://doi.org/10.1029/2020jd034400, 2021.

Zuanon, N.: IceCube, a portable and reliable instrument for snow specific surface area measurement in the field, International Snow Science Workshop, pp. 1020–1023, www.A2PhotonicSensors.com, 2013.

Zuhr, A. M., Münch, T., Steen-Larsen, H. C., Hörhold, M., and Laepple, T.: Local-scale deposition of surface snow on the Greenland ice sheet, The Cryosphere, 15, 4873–4900, https://doi.org/10.5194/tc-15-4873-2021, 2021.